TM-X-72611

77-01

National Space Science Data Center/
World Data Center A For Rockets and Satellites

A Model of the Near-Earth Plasma Environment

and

Application to the ISEE-A and -B Orbit

July 1977

NSSDC/WDC-A-R&S 77-01

A Model of the Near-Earth Plasma Environment and Application to the ISEE-A and -B Orbit

by

King W. Chan
Donald M. Sawyer
James I. Vette

July 1977

National Space Science Data Center
National Aeronautics and Space Administration
Goddard Space Flight Center
Greenbelt, Maryland 20771

CONTENTS

APPENDIXES

TABLES

ILLUSTRATIONS

I. INTRODUCTION

The purpose of this report is to present a model of the near-Earth environment and use it to obtain a best estimate of the average flux of protons and electrons in the energy range from 0.1 to 100 keV for the International Sun-Earth Explorer (ISEE)-A and -B spacecraft. This report is the result of a study initiated by a concern for the possible radiation damage to the thermal coating on these spinning spacecraft, both of which will be placed in a geocentric orbit with initial apogee of 21 R_E, perigee of 280 km, and inclination of 28.5°. Applications of the model to other high-altitude satellites can be obtained with the appropriate orbit averaging.

To the best of our knowledge, this is the first attempt to synthesize an overall quantitative environment of low-energy particles for high-altitude spacecraft, using data from in situ measurements. In formulating model environments of the more energetic ($\gtrsim$ 100 keV) particles trapped in the radiation belts of the Earth (e.g., *Sawyer and Vette*, 1976), the spatial cells used are small volumes of the tubes of force formed by the geomagnetic field. However, the general morphology of the near-Earth plasma dictates a much grosser spatial structure in which the average particle fluxes need to be obtained. The appropriate spatial regions for the plasma environment consist of various parts of the magnetosphere and the interplanetary medium in which the character of the low-energy particles and the magnetic field have provided a natural identification. Within these regions, there are large spatial and temporal variations.

The five spatial regions (interplanetary medium, magnetosheath, plasma sheet, high-latitude magnetotail, and inner magnetosphere) have been chosen as the spatial structure for the present study. Since the real geometries of these regions do vary with time, model boundaries for the regions must be used; then, the average character of the fluxes within each region must be ascertained. In the application of this environment, the final objective is to derive an orbit-averaged, differential energy, spin-averaged spectra for protons and electrons. To obtain the best available environment, all quantitative high-altitude satellite measurements published in the literature have been considered, regardless of the energy or angular resolution of the instrument. Data from low-altitude, polar-orbiting spacecraft have not been included. Publications of qualitative data will be referenced to confirm the trend of the quantitative results. Only fluxes that are long-term or reported as typical will be included. Short-term, transient phenomena will generally be neglected, unless they make an obvious and significant contribution to the average environment. No attempt will be made to give a comprehensive review of the physics associated with these low-energy particles.

The basic approach employed in the derivation of the orbit-averaged spectra is divided into two steps. In the first step, published spectra

belonging to each of the five regions are compiled, and a composite spectrum representing the environment of that region is constructed. In cases where there are substantial differences in data from several measurements, spectra of a high estimate, as well as a low estimate, are determined. The details will be given in Section III. In the second step, the composite spectra of each region are weighted according to the fraction of the orbital time the spacecraft is located in the corresponding region. As the orbits precess about the north ecliptic pole, the weighting factor of each region changes. The details of the second step, using the first 6 months of the planned ISEE-A/-B orbit, will be described in Section IV.

To date, the abundance of the published data and the completeness of documentation for various regions cannot be viewed with the same standard. Because of the nature of the plasma characteristics, and perhaps because of the focus of interest in the scientific community, the solar wind in the interplanetary medium is the best documented region, while the magnetosheath has comparatively few publications with quantitative data in absolute flux units. Accordingly, the resultant spectra of one region may have an uncertainty factor quite different from that of the spectra of other regions.

As previously noted, the particle properties are distinctively different in the various spatial regions. Often, it is necessary to use simplifying assumptions to derive representative spectra for a particular region. The data on the solar wind proton bulk flow, for example, require the computation of time- and spin-averaged fluxes. Details of the mathematics will be given in the Appendixes.

II. THE SPATIAL STRUCTURE FOR THE NEAR-EARTH PLASMA ENVIRONMENT

For the purpose of flux averaging along a given orbit, it is essential to identify the positions of the spacecraft with respect to those regions of the near-Earth environment that have distinctively different particle populations. The International Magnetospheric Study/Satellite Situation Center (IMS/SSC) has developed a computer program that can merge a model configuration of the magnetosphere with the ephemeris of an Earth-orbiting satellite (*Vette et al.*, 1976). This program has direct application in the present study.

In a report presented at the 10th ESLAB Symposium, (*Vette et al.*, 1976), eight regions of the near-Earth space were defined by the simple boundaries that are listed in Table 1. Fairfield's model (*Fairfield*, 1971) was used for the boundary locations of the bow shock and the magnetopause. Some of these regions are illustrated in Figure 1. This classification of space is intended to provide a general frame of positions for the study of particles and fields in the IMS.

Because of the lack of sufficient low-energy particle data to establish distinctively different statistics for a local time effect in the magnetosheath and the inner magnetosphere, the further separation of these two regions into dayside and nightside regions has been eliminated in the present study. Furthermore, the midlatitude magnetotail and the neutral sheet have been combined and named the plasma sheet, which is a popular term in the literature for the low-energy particles found in this region. As a result of this slight modification, only five regions as defined in Table 1 have been used; the previously noted IMS/SSC computer program is still applicable without change.

III. DERIVATION OF COMPOSITE SPECTRA

A. The Interplanetary Medium

The low-energy particle environment in the interplanetary medium near the Earth is dominated by the "quiet" solar wind. Since most of the solar wind observations found in the literature are described in terms of fluid parameters (temperature, density, and bulk flow speed), they must be converted to a differential energy flux; the method is given in Appendix A. Short-term variations in the interplanetary fluxes can be associated with transient solar activity. These include flare particle events, fluxes associated with active regions, and interplanetary shock-associated spikes (for a review, see *Lin*, 1974b). Shock-associated spikes, with a duration on the order of minutes, will not appreciably affect the average environment and are not considered in this study. The presence of the Earth and its magnetosphere can also add to the near-Earth, interplanetary environment through reflection and emission of particles at the bow shock (*Asbridge et al.*, 1968; *Frank*, 1970b; *Lin et al.*, 1974).

The directionality of the various interplanetary fluxes varies widely and must be taken into account in the construction of a useful composite spectrum. The electron and proton components of the "quiet" solar wind are distinctly different in this regard. For the electron flux, the nearly isotropic thermal component of velocity is large compared with the bulk flow component that is commonly referred to as the solar wind velocity. For protons, the opposite situation is obtained in that the thermal component is small compared to the bulk flow component. Thus, the electrons in the solar wind are essentially isotropic, while the protons are highly anisotropic. (For reviews, see *Montgomery*, 1972; *Wolfe*, 1972.) Typically, the protons arrive within a cone of 20°, centered along the bulk flow direction (*Hundhausen et al.*, 1967). In addition, the magnitude of the bulk flow speed varies within the approximate range of 250 to 700 km/s. To compare this flux with that from other regions of space where fluxes are more nearly isotropic, a time- and spin-averaged, solar wind proton flux is constructed. This approach will be discussed more fully in the following paragraphs. Details are given in Appendixes B and C.

A typical low-energy, solar wind electron spectrum, with a density equal to 9 cm^{-3} and a temperature equal to 1.5×10^5 K, is shown in Figure 2 (*Montgomery et al.*, 1968; *Montgomery*, 1972). Also shown is a portion of the quiet-time composite spectrum (*Lin et al.*, 1972), which extends over 12 decades of flux for energies up to 100 keV. IMP 6 observations during a "quiet" period and during an anisotropic flare packet (*Frank and Gurnett*, 1972) are also shown. The remaining spectra from OGO 5 (*Ogilvie et al.*, 1971), IMP 4 and IMP 6 (*Wang et al.*, 1971), Apollo 15 subsatellite (*Lin*, 1974a), and the Apollo 16 subsatellite (*Lin et al.*, 1973a) were all obtained during various flare events. These events have been observed for energies as low as 1 keV.

From this compilation of spectra, a representative isotropic composite spectrum has been constructed and is also shown in Figure 2. Without a statistical study of the flare spectra at energies above 1 keV, it is difficult to determine their contribution to the average environment. However, by extending the quiet-time observation of IMP 6 (*Frank and Gurnett*, 1972) to higher energies, a reasonable estimate of the flare contributions to the quiet-time composite of *Lin et al.* (1972) is obtained. The IMP 6 spectrum at lower energies joins smoothly with the Lin composite spectrum; and, therefore, they are used as the basis for the isotropic composite spectrum below 1 keV. Also shown is a spectrum representing the maximum anisotropic flare fluxes observed.

An interplanetary medium, quiet-time proton spectrum for energies above 38 keV is shown in Figure 3 (*Lin et al.*, 1973b). Also shown is a derived, interplanetary medium, average proton spectrum based on enhanced fluxes associated with solar active regions and flares. This spectrum is three orders of magnitude below the IMP 6 proton fluxes seen propagating upstream from the bow shock with energies above 30 keV (*Lin et al.*, 1974). These IMP 6 protons are observed when the spacecraft is on an interplanetary magnetic field line that intersects the bow shock. In the energy range from 6 to 40 keV, IMP 4 has observed transient events, which *Frank* (1970b) has identified as magnetic storm-associated fluxes. They were quasi-isotropic in the ecliptic plane but favored intensities arriving from the solar direction by factors of two to three. A nonstorm upper limit from IMP 4 for energies in the range of 11 to 18 keV is also shown in Figure 3. Protons propagating out from the bow shock along interplanetary field lines have been observed by IMP 4 (*Frank*, 1970b). These particles, shown in Figure 3, are quasi-isotropic over a hemisphere looking toward the bow shock and have energies in the range 0.2 to 4 keV. However, for energies below about 4 keV and looking in the solar direction, the solar wind dominates.

The proton component of the solar wind can be characterized as a highly anisotropic beam of particles with a narrow energy spread. The peak flux occurs at an energy close to that given by a proton moving with the bulk solar wind speed. Two examples of instantaneous solar wind proton spectra, corresponding to bulk speeds of 300 and 700 km/s, are shown in Figure 3. Over a period of time, the solar wind speed ranges between 250 and 700 km/s. Derived density and temperature parameters are found to correlate with the solar wind speed (for a review, see *Wolfe*, 1972). Using observations from Vela 3A and 3B obtained during the period July 1965 to November 1967 (*Hundhausen et al.*, 1970), it is possible to derive a time-averaged, solar wind spectrum. This spectrum is shown in Figure 3, and additional details of the derivation are given in Appendix B. Although this spectrum is derived using a distribution for solar wind speeds obtained near solar minimum and during a rising portion of the solar cycle, distributions obtained during other phases of the solar cycle are only expected to change the average spectrum slightly. The highly anisotropic nature of this spectrum makes it difficult to compare with the other, more isotropic fluxes. To resolve this difficulty, an effective spin-averaged, isotropic spectrum has been generated and is shown

in Figure 3. An area that is oriented perpendicular to the ecliptic plane and spinning about an axis that is also perpendicular to the ecliptic plane, will receive the same average flux from this spectrum as it would from the anisotropic, time-averaged, solar wind spectrum. The derivation of this spin-averaged spectrum is given in Appendix C. Similarly, a spin-averaged, bow shock spectrum has been constructed by smoothly joining the two bow shock-related spectra and then dividing the flux by two to account for the quasi-isotropic nature of these fluxes over one hemisphere. The resulting spin-averaged, bow shock spectrum is shown in Figure 3.

A composite proton spectrum for the interplanetary medium near the Earth now can be constructed by adding together the spin-averaged, solar wind and bow shock proton spectra. This spectrum, shown in Figure 3, is isotropic and simulates the effect of the observed anisotropic spectra on a plane area that is spinning as previously described. This is approximately the geometry for a unit area on the side of the spinning ISEE-A/-B spacecraft.

B. The Magnetosheath

The magnetosheath is the region between the bow shock and the magnetopause as shown in Figure 1. The bow shock is the boundary defined observationally by the abrupt changes that occur in the characteristics of the plasma and the magnetic field (*Montgomery et al.*, 1970). The magnetopause is the boundary formed by the geomagnetic field as a standoff limit to the solar wind plasma from the interplanetary medium.

In the magnetosheath, the post-shock plasma from the solar wind flows around the magnetosphere and is usually turbulent (*Hundhausen et al.*, 1969; *Scudder et al.*, 1973). For the low-energy particles in this region, the presentations of information in the literature are generally divided into two groups: (1) in the form of differential spectra constructed directly from the observed fluxes (e.g., *Frank*, 1970a; *Rosenbauer et al.*, 1975); and (2) in terms of particle distribution functions and moments expressed as conventional fluid parameters that are also derived from the observed fluxes (e.g., *Hundhausen*, 1970). When available, data obtained in absolute flux units will be used for analysis.

Figure 4 shows the electron spectra measured by the Vela 4B, IMP 5, and Apollo 14 spacecraft with the source publication listed in the figure legend. The Apollo 14 data are given to show that the electron spectra in the distant magnetosheath (~60 R_E) are similar to those observed by Vela 4B at about 18 R_E.

Because of the lack of comparable statistical information about these measurements, there is no simple way that the various spectra can be properly weighted to construct a single, smooth spectrum. For the present purpose of making a crude, quantitative projection of the environment, an

upper-bound and a lower-bound envelope are constructed as the composite spectra for a high and low estimate. As shown by the dashed lines in Figure 4, the composite spectra are generally broader than any of the individual, measured spectra. Given the uncertainty as represented by the range of variations in the estimates, the composite spectra can be regarded as representing the long-term, average fluxes in the region.

As is the case for electrons in the interplanetary medium, the angular distribution of the magnetosheath electron fluxes shows relatively little variation (within a factor of two) with respect to the bulk flow direction (*Montgomery et al.*, 1970). Therefore, no spin averaging is needed for the present flux estimates.

Figure 5 shows the magnetosheath proton spectra observed by the HEOS 1, HEOS 2, IMP 4, and IMP 5 satellites. For the low-energy protons in this region, the bulk flow velocity is a major contributing factor in the observed kinetic energies of the particles (*Hundhausen et al.*, 1969). The proton flux, therefore, is highly anisotropic with the peak flux in the direction of the bulk flow as shown by the HEOS 2 measurements at three azimuthal angles in Figure 5. However, in comparison with the protons in the interplanetary medium discussed previously, the protons in the magnetosheath generally have a lower bulk flow speed and a higher mean thermal velocity. Consequently, the angular distribution of the low-energy protons is less anisotropic in the magnetosheath than in the interplanetary medium. In addition, proton spectra in the magnetosheath show considerably more deviation from a Maxwell-Boltzmann distribution than in the case of the interplanetary medium (*Formisano et al.*, 1973).

As previously described for the case of electron spectra in the magnetosheath, an upper-bound and a lower-bound envelope are constructed to serve as composite spectra representing a high estimate and a low estimate in the presumed flow direction. Because the composite spectra are generally broader than any of the individual, observed spectra, the result of the estimated flux, when integrated over all energies, will be conservatively higher than the average situation. However, the differential flux from the composite spectrum at a given energy will probably be comparable to the average measurement within the range of uncertainty as indicated by the high and low estimates.

In order to calculate the averaged proton fluxes received by a unit area of a spinning surface with the spin axis perpendicular to the ecliptic plane, both the flow component as well as the thermal component of the particle velocity must be considered in the angular integration and the spin-averaging processes. In practice, as described in detail in Appendix D, it is convenient to make the calculation using an analytic distribution function that fits the composite spectra.

In general, the K-distribution function with K = 2 (*Formisano et al.*, 1973) is found to give a reasonable fit to a typical, observed proton

spectrum in the magnetosheath. In the present analysis, the composite proton spectra of the magnetosheath can be well approximated by the K-distribution with a bulk flow speed of 230 km/s, thermal energy (kT) of 400 eV, and a density of either 17 cm^{-3}, or 2 cm^{-3} for the high and low estimates, respectively.

The results of the calculation (see Appendix D for details) are presented in Figure 6. The effective isotropic spectra shown in the figure give the equivalent isotropic environment that the previously specified surface area will encounter in orbit. They can be used to compare with other isotropic spectra for the purpose of making flux estimates on this area, but they cannot be used for other purposes such as calculating an omnidirectional flux. A procedure for correctly deriving an omnidirectional flux spectrum is included in Appendix D.

C. The Inner Magnetosphere

The inner magnetosphere, shown as region C in Figure 1, is composed of the entire dayside magnetosphere and that part of the nightside magnetosphere where the absolute value of the X-coordinate is less than 10 R_E in the geocentric solar ecliptic (GSE) coordinate system. A further restriction for this study is the consideration of only near-equatorial latitudes. This large, asymmetric volume, which includes the inner and outer radiation belts, is known to contain a sea of protons and electrons with energies in the range 100 eV to 50 keV (cf., *Vasyliunas*, 1972). Observations of the electrons are considerably more complete than those of the protons, but even they are lacking in spectral, temporal, and spatial coverage. This is in part a result of background problems, some of which arise from the presence of higher energy particles and solar ultraviolet radiation (*Gringauz*, 1969), and some not yet clearly identified (*Lyons and Williams*, 1976). Nevertheless, the general picture for electrons is one of considerable spatial structure and temporal variation in the flux of this region. (For reviews, see *Gringauz*, 1969; *Vasyliunas*, 1972.)

It is more difficult to characterize the proton population in the inner magnetosphere since there are few observations covering the more distant parts of the dayside region beyond an L (McIlwain parameter) of about 7. OGO 3 observations (*Frank and Owens*, 1970) have provided a survey of low-energy protons in the evening to midnight quadrant. (For reviews, see *Frank*, 1970; *Vasyliunas*, 1972.) Protons in the plasma sheet continue across the inner boundary of the plasma sheet up to the plasmasphere. The evening plasma sheet boundary, as identified in the electron flux, is not observable in the proton flux. These protons are most intense in the evening sector, forming the quiet-time, proton ring current centered near L = 6.5. During storms, the intensity of these protons greatly increases, forming the storm-time ring current (cf., *Frank*, 1967b).

In addition, the dayside magnetosphere boundary (magnetopause) has been observed to contract significantly inward during large geomagnetic storms. The greatest observed contraction to date was associated with the storm of August 2, 1972, when the magnetopause was reported to be inside the Explorer 45 satellite position at L = 5.2 (*Hoffman et al.*, 1975). The effects of such a contraction on the particles normally residing outside the synchronous orbit (L ~ 6.6) have not yet been observed but are certainly significant.

Vasyliunas (1972) has described the spatial structure of the electron fluxes with energies from 100 eV to a few keV. These electrons are found within the equatorial region of the magnetotail, where they form the plasma sheet. These intense fluxes terminate abruptly where they define the inner boundary of the plasma sheet in the evening side of the magnetosphere. This occurs at about 11 R_E during "quiet" times. This boundary approaches the plasmasphere (~6 R_E) near the midnight meridian. Moving from evening to earlier, local times, this boundary remains at ~11 R_E and, finally, intersects the magnetopause near noon. Weak electron fluxes are observed between the plasma sheet and the plasmasphere in the evening sector. They are observed to be an order of magnitude or more below those in the plasma sheet at a few keV (*Schield and Frank*, 1970). They grow stronger as one moves to earlier, local times and expand in spatial extent until they fill the entire region between the magnetopause and the plasmapause near noon. In the morning sector, the fluxes show a strong radial gradient, increasing toward the magnetopause. In the predawn hours, the fluxes become very intense and extend all the way from the magnetopause in to the plasmapause. At these local times, they are an order of magnitude larger than at other local times. These fluxes must then decrease as one moves toward midnight so as to merge with the plasma sheet. During substorms, the plasma sheet boundary moves toward the Earth in the evening sector. It is, therefore, apparent that the inner magnetosphere will also contain appreciable plasma sheet electrons that must be included in the generation of a composite electron spectrum for this region.

Figure 7 is a representative compilation of the differential electron spectra available in the literature. OGO 1 (*Vasyliunas*, 1968) and OGO 3 (*Frank*, 1967c; *Schield and Frank*, 1970) spectra were obtained in the evening and midnight sectors, respectively. The OGO 3 spectra in the plasma sheet at L = 9.8 and in the edge of the plasma sheet at L = 9.25 are more than an order of magnitude higher than the electron trough spectrum at L = 8.8 for energies of a few keV. At L = 5.3 (in the plasmasphere) and at L = 3.9, the spectra are between those at L = 8.8 and L = 9.8 for energies of a few keV. At the lower energies, they continue to rise, while the plasma sheet spectra appear to fall. The OGO 1 spectrum was obtained during a substorm and shows the typical plasma sheet spectrum extending over the evening region from 7 to 11 R_E. At this time, the 5-R_E spectrum has the appearance of the OGO 3 trough spectrum. The Hawkeye 1 spectrum at L = 5.8 (*Garnett and Frank*, 1976) and the Electron 2 spectrum at L = 8 (*Vernon et al.*, 1966) were both obtained in the morning

sector and are consistent with the radial gradient previously discussed. In association with a large magnetic disturbance, the Hawkeye 1 spectrum was observed to be an order of magnitude larger than the more typical spectrum shown in Figure 7. The Explorer 45 spectrum at L = 5.2 (*Lyons and Williams*, 1975) and the ATS 5 spectrum at L = 6.6 were observed in the evening sector. These spectra were about an order of magnitude below the OGO 3 spectrum at L = 5.3. At 10 keV, the ATS 5 spectrum (*Barfield et al.*, 1977) is more than a factor of 50 below the other spectra. During a substorm, the ATS 5 spectrum increased two orders of magnitude for energies in the range of 10 to 20 keV. These differences are indicative of the spatial and temporal variations that can occur.

The average outer zone integral electron spectrum from the AE-4 model (*Singley and Vette*, 1972), for L in the range 6 to 8, has been differentiated and included to show the trend above 50 keV. The corresponding spectrum for L = 10 would be about an order of magnitude lower at these energies.

From this compilation of spectra, a single composite spectrum to represent this region has been constructed and is shown in Figure 7. At energies above 10 keV, this spectrum is constructed to lie above most of the observations and still be within a factor of two or three of an average of the observations. At energies between 1 and 10 keV, this spectrum is constructed to represent an average between the intense fluxes encountered in the plasma sheet and predawn hours and the much lower fluxes observed in the electron trough region for late afternoon and evening hours. At energies below 1 keV, this spectrum is constructed to reflect the rising trend of the OGO 3 data at L = 3.9, 5.3, and 8.8. Although the plasma sheet spectra appear to be falling at these energies, the lack of sufficient local time coverage requires a more conservative approach in this energy range. This composite spectrum can be assumed to be isotropic for the purposes of radiation damage studies. The error associated with this approximation is small compared to the uncertainties associated with the spatial and temporal variations.

Figure 8 is a representative compilation of the differential proton spectra available in the literature. All spectra were obtained in the early evening to midnight quadrant, except for the synchronous OV2-5 spectrum (*Stevens et al.*, 1970) obtained at noon with L ≈ 6.6. The corresponding midnight spectrum at synchronous altitude was about a factor of four lower for energies in the 60 to 100 keV range. The OGO 3 observations at L = 3.9, 6, and 11.8 (*Frank*, 1967c) can be associated with the plasmasphere, ring current and plasma sheet, respectively, during "quiet" times. The effect of a geomagnetic storm on the OGO 3 observations at L = 4, 6, and 7.1 is also shown. The increased flux at L = 4 in the 10- to 40-keV range is an observation of the storm-time ring current. An average spectrum, obtained from OGO 3 during June and July 1966, is shown for L = 4.5 and L = 6 (*Pizzella and Frank*, 1971). There are considerable differences below 4 keV between these average spectra and the single

observations at L = 3.9 and 6 discussed earlier. These differences are assumed to be indicative of the temporal variations. The Explorer 45 observations at L = 4.25 (*Smith et al.*, 1976) and L = 4.6 (*Williams et al.*, 1973) correspond to relatively "quiet" conditions. The perpendicularly mirroring flux at L = 4.25 was about a factor of 25 higher at 30 keV during the main phase of a geomagnetic storm. The two ATS 5 spectra (*DeForest*, 1972) at synchronous altitude (L ≈ 6.6) correspond to near-loss cone and near-equatorially mirroring fluxes in the evening sector. The similar magnitudes of these two spectra indicate a nearly isotropic flux. As was the case for the electrons, the error in assuming isotropy will be small compared to the other uncertainties.

A single composite spectrum was derived from these observations and is also shown in Figure 8. This spectrum follows the upper range of the quiet-time observations for energies above 1 keV. Below 1 keV, the spectrum follows the rising trend of the spectra at L = 3.9 (OGO 3), 4.25 (Explorer 45), and 4.6 (Explorer 45). This should provide a conservative representation of this energy range, especially in view of the divergence of trends below a few keV.

D. The Plasma Sheet

In the model configuration of the near-Earth space described in Section II, the plasma sheet is a nightside region centered about the midplane of the magnetotail with a thickness of 12 R_E. At a radial distance of 18 R_E from the Earth, Vela satellite measurements have shown the same thickness for the plasma sheet near the dawn and dusk edges of the magnetotail (*Akasofu et al.*, 1973). However, the Vela satellites observe that the apparent thickness of the region gradually reduces to about 6 R_E near the local midnight meridian. Since the plasma intensity in the adjacent high-latitude magnetotail is comparatively much lower than in the plasma sheet, an overestimate of the size of this region will give a conservative estimate of the fluxes in this part of space.

Figures 9 and 10 show the low-energy proton and electron data recorded by the Vela 3B, Vela 4B, and OGO 3 satellites during the 1965 to 1968 time period. It is noted that the Vela 4B spectra in Figure 10 are composites that are based on a set of five spectra published by *Hones et al.* (1972). All the spectra used in this study are classified as typical plasma sheet protons or electrons by the experimenters. Effects of substorms and isolated localities of acceleration or injection are regarded as transient phenomena and have been tentatively excluded.

It can be seen in Figures 9 and 10 that the spectra, as observed by different satellites or at different times, are quite variable in energy range as well as in flux level. Similar to the case of the magnetosheath, high and low estimates are constructed to serve as composite spectra and

are shown by the dashed lines in Figures 9 and 10. The area enveloped by the composite spectra represents the range of uncertainty in the estimates.

There have been reports that the protons in the plasma sheet form enhanced flows (e.g., *Hones et al.*, 1972, 1973, 1974) during magnetospheric substorms and sometimes produce explosive jet streams (called "fireballs") in some localities in the magnetotail (*Frank et al.*, 1976). However, with the exception of these occasional events during substorms, the fluxes of low-energy protons and electrons in the plasma sheet have been characterized as "most often isotropic" (*Akasofu et al.*, 1973; *Bame et al.*, 1967). Because only long-term effects are of major concern in the present study, no spin averaging is required, and all fluxes are taken to be isotropic.

E. The High-Latitude Magnetotail

The plasma intensity in the high-latitude magnetotail is generally very low during "quiet" times. It is usually below the detection threshold of the instrument or below the cosmic-ray background level. The Vela electrostatic analyzer, for example, can only measure the electron flux in the region, but cannot record the proton flux during nonstorm time, because the proton count rate is below the count rate produced by the cosmic rays in the instrument (*Akasofu et al.*, 1973). Comparatively, the Vela instruments have documented very extensive data of both electrons and protons for the plasma sheet region previously discussed.

In fact, there are only two spectra published in units of differential flux available in the literature for the high-latitude magnetotail region: one for protons from an IMP 4 measurement (*Frank*, 1970a), and one for electrons from Vela 5B, 6A, and 6B observations (*Akasofu et al.*, 1973). These two spectra, shown in Figure 11, have already been quoted as representative spectra in many review articles (e.g., *Vasyliunas*, 1972; *Frank*, 1970a; *Wolfe and Intriligator*, 1970).

The shapes of the spectra in this region are similar to those found in the magnetosheath, but the flux level is much lower than in the magnetosheath. The high-energy skew of the proton spectrum above 2 keV resembles in shape the skew of the reported ring current protons. (For a review, see *Vasyliunas*, 1972.)

Isotropic angular distributions for the fluxes of protons and electrons in this region are reported as a usual feature (*Frank*, 1970a; *Akasofu et al.*, 1973); and, therefore, no spin averaging is needed.

The validity of these spectra in the high-latitude magnetotail is limited to a radial distance below 22 R_E. The high-latitude magnetotail at lunar distances of 60 R_E, for instance, can have quite different characteristics (*Hardy et al.*, 1976).

As previously noted in Section II, a region of relatively less extent just inside the magnetopause, named the plasma mantle (*Rosenbauer et al.*, 1975) or boundary layer (*Akasofu et al.*, 1973), has not been treated separately in the present study. The particles in this boundary layer have been observed to have the characteristics between that of the magnetosheath and the plasma sheet. Since this layer is very thin, less than 1 R_E in most cases, it is expected that the omission of this region will not substantially affect the accuracy of the present study.

F. A Summary of the Composite Proton and Electron Spectra

Composite proton spectra from the five regions are shown in Figure 12. High and low estimates are given for the spin-averaged, magnetosheath spectra and plasma sheet spectra. The high-estimates, corresponding to envelopes of observed differential fluxes, will give an overestimate or upper bound to the integral fluxes. Similarly, the low estimates yield a lower bound for the integral fluxes. The high-estimate magnetosheath proton spectrum has the highest fluxes for energies in the range 100 eV to 6 keV; while above 6 keV, the inner magnetosphere spectrum dominates. The spin-averaged, interplanetary proton spectrum, which includes the time-averaged, solar wind spectrum, shows significant fluxes in the energy range from about 300 eV to 3 keV. The high-energy, interplanetary tail, with energies above approximately 4 keV, corresponds to protons propagating upstream from the bow shock. Its presence is dependent on the satellite location and interplanetary magnetic field orientation. The plasma sheet spectra tend to be an order of magnitude or more below those of the magnetosheath, while the high-latitude magnetotail spectrum is about an order of magnitude below those in the plasma sheet.

It should be noted that the interplanetary and magnetosheath spectra are not true isotropic fluxes; therefore, a true omnidirectional flux cannot be obtained by multiplying by 4π. However, the flux [protons/$(cm^2 \cdot s \cdot eV)$] through an area oriented perpendicular to the ecliptic plane and spinning can be obtained by multiplying any of the spectra in Figure 12 by π.

Composite isotropic electron spectra from the five regions are shown in Figure 13. The high-estimate plasma sheet spectrum and the inner magnetosphere spectrum show comparable fluxes for energies above 200 eV. Below 200 eV, the high-estimate magnetosheath spectrum and the inner magnetosphere spectrum show comparable fluxes. The interplanetary spectrum is nearly identical with the low-estimate magnetosheath spectrum for energies above 50 eV, while the high-latitude magnetotail spectrum is one to three orders of magnitude below the other spectra.

The relative importance of a spectrum from a particular region, in regard to its radiation damage potential, depends on the satellite orbit. As an example, Section V describes the application of this environment to the ISEE-A/-B orbit.

IV. THE ISEE-A/-B ORBIT

As introduced earlier, Figure 1 shows the projection of the model magnetosphere and some of the revolutions of the ISEE-A/-B orbit rotated into the X-Y plane of the GSE coordinate system. The schematic definition of the five spatial regions is also shown in the figure. Because the Z-axis is not shown, regions D and E are represented by the same area in the X-Y projection. Of particular interest, in this case, is the evolution of the orbital position with respect to the various spatial regions. Starting from launch on Day 288, 1977, the spacecraft crosses the bow shock until late January 1978. It enters the high-latitude magnetotail in late February of the same year. About 6 months after launch, the apogees of ISEE-A/-B precess 180° from the dayside to the nightside of the magnetosphere.

Figure 14 shows the details of the first 6 months of orbital time in which ISEE-A/-B are located in various regions. It can be seen that the major regional contributions to the orbit come first from the interplanetary medium; then from the magnetosheath plus the inner magnetosphere; and, finally, from the plasma sheet and the high-latitude magnetotail. When the orbit-averaged spectra are calculated, the fraction of orbital time in each region is used as the weighting factor for that region. Results of these computations are presented in Section V.

As previously noted, the classification of spatial regions is limited by the constraints of the current computing programs and the availability of the low-energy particle data. Some areas of relatively less extent but of considerable scientific significance, such as the plasma mantle or boundary layer, are omitted in the present version of the environmental estimate.

V. THE APPLICATION OF THE ENVIRONMENT TO THE ISEE-A/-B ORBIT

The number of days per revolution in a given region for each of the first 76 ISEE-A/-B revolutions is shown in Figure 14. This group of revolutions comprises approximately 6 months and corresponds to an apogee precession from late morning to near midnight. This sample of revolutions can be used to generate an average revolution in which the spacecraft spends a certain percentage of its time in each of the five regions. Weighting each region spectra by the corresponding percentage of time spent in the region and summing the resultant spectra yields an orbit-averaged spectrum. Figures 15 and 16 show the results of this analysis for the ISEE-A/-B orbit as applied to the proton and electron spectra, respectively. The percentage of time spent in each region is indicated in both figures along with the weighted spectra and the final orbit-averaged spectrum. Most of the time is divided among regions of the inner magnetosphere (32 percent), interplanetary medium (25.2 percent), and magnetosheath (20.8 percent); while little time is spent in the plasma sheet (12 percent) and high-latitude magnetotail (10 percent). In order not to underestimate the final fluxes, the high-estimate spectra were used when available.

It is apparent from Figure 15 that the magnetosheath is the major contributor to the average proton spectrum for energies below 5 keV, while the inner magnetosphere is the major contributor at higher energies. If the low estimate had been used for the magnetosheath, the average spectrum would have been reduced less than a factor of three for energies below 5 keV and an insignificant amount at higher energies.

The corresponding analysis for the electron spectra is shown in Figure 16. Approximately half of the average spectrum is derived from the inner magnetosphere. The remaining half is contributed by the high-estimate magnetosheath spectrum for energies below 300 eV and by the high-estimate plasma sheet spectrum for energies above 300 eV. If the low-estimate spectra for the magnetosheath and plasma sheet had been used, the average electron spectrum would have been reduced less than a factor of two.

The significance of the inner magnetosphere proton and electron spectra for energies in the range 100 eV to 100 keV is now apparent. As discussed in Section III, this region is characterized by large spatial and temporal variations for low-energy particles. It is likely that the composite spectra for this region overestimate the average situation, but it is difficult to say by what factor. More observations, on the dayside particularly, are needed.

The orbit-averaged proton and electron differential energy spectra from Figures 15 and 16 are compared in Figure 17. The differential flux [protons/(cm^2•s•eV)] through a unit area, oriented perpendicular to the

ecliptic plane and spinning, may be obtained by multiplying the spectra in Figure 17 by a factor of π. If the radiation damage expected from these particles is not strongly energy dependent, it is useful to have integral flux values. These values have been calculated by integrating the spectra of Figure 17 from a given energy up to 10^5 eV and then multiplying by π to convert to units of integral area flux (J_A) as shown in Figure 18. An omnidirectional electron flux can be obtained by multiplying J_A by a factor of four. An omnidirectional proton flux cannot be calculated directly from J_A, because the solar wind and magnetosheath proton spectra are highly anisotropic. Appendix C gives the procedure for an analytic calculation of the omnidirectional flux when the particle fluxes can be represented by a Maxwell-Boltzmann distribution moving with a bulk speed. A similar procedure for use with a K-distribution is given in Appendix D. As an aid to the user, Table 2 contains numerical values for the spectra shown in Figures 17 and 18.

Appendix A. The Conversion From Fluid Parameters to Energy Spectra

It is sometimes possible to represent a particle population by an analytic function employing only a few parameters that have physical significance. One such function is the Maxwell-Boltzmann distribution, which is characterized by parameters of density (n) and temperature (T) (e.g., *Sears*, 1953). The Maxwell-Boltzmann phase space density distribution function f_m can be written as

$$f_m = n \left(\frac{m}{2\pi kT}\right)^{3/2} \cdot e^{-\frac{mv^2}{2kT}} \qquad (A.1)$$

where f_m is the number of particles per unit (position) volume and per unit velocity volume, having (thermal) speed v; m is the particle mass; k is the Boltzmann constant; T is a characteristic temperature; and n is the number of particles per unit volume.

Another function that has been found to be useful is referred to as the K-distribution, which can be written as

$$f_K = \frac{nK!}{K^{3/2}\,\Gamma(K-\frac{1}{2})\pi^{3/2}\,W^3} \cdot \frac{1}{\left(1+\frac{v^2}{KW^2}\right)^{K+1}} \qquad (A.2)$$

where Γ is the gamma function, W is a thermal speed characterizing the distribution, K is an integer, and the other variables are as previously given. In the limit of K approaching infinity, f_K becomes the Maxwell-Boltzmann distribution f_m. *Formisano et al.* (1973) have defined a K-distribution temperature T in terms of W using the relation

$$kT = \tfrac{1}{2}mW^2 \left(\frac{K}{K-\frac{3}{2}}\right) \qquad (A.3)$$

The two distributions given by (A.1) and (A.2) do not have an explicit angular dependence.

Given a general phase space density distribution f, it is useful to determine the corresponding differential-energy unidirectional flux j.

Expressing these quantities in terms of differential elements yields

$$f = \frac{dN}{dx\ dy\ dz\ dv_x\ dv_y\ dv_z} \tag{A.4}$$

$$j = \frac{dN}{d\Lambda\ dt\ d\Omega\ dE} \tag{A.5}$$

where N is the number of particles; x, y, z are position coordinates; v_x, v_y, v_z are velocity coordinates; Λ is an area, t is a time, Ω is a solid angle, and E is an energy. By transforming the differential volume elements to give

$$dv_x\ dv_y\ dv_z = v^2\ d\Omega\ dv \tag{A.6}$$

$$dx\ dy\ dz = d\Lambda\ dz = d\Lambda\ v_N\ dt \tag{A.7}$$

where v_N is the component of particle velocity perpendicular to area $d\Lambda$, f can be written as

$$f = \frac{1}{v_N v^2} \cdot \frac{dN}{d\Lambda\ dt\ d\Omega\ dv} \tag{A.8}$$

By restricting $d\Omega$ to be perpendicular to $d\Lambda$, v_N can be replaced by v. Differentiating the nonrelativistic particle kinetic energy

$$E = \tfrac{1}{2}mv^2 \tag{A.9}$$

to obtain

$$dE = mv\ dv \tag{A.10}$$

and substituting into (A.8), yields

$$f = \frac{m}{v^2} \cdot \frac{dN}{d\Lambda\ dt\ d\Omega\ dE} = \frac{m}{v^2} j \tag{A.11}$$

where j is the desired flux as given in (A.5). The general result of

$$j = \frac{v^2}{m} f \tag{A.12}$$

can now be used with (A.1) to give the isotropic Maxwell-Boltzmann energy spectrum j_m:

$$j_m = \frac{n m^{1/2} v^2}{(2\pi kT)^{3/2}} \cdot e^{-\frac{mv^2}{2kT}} \tag{A.13}$$

In the solar wind and in the magnetosheath, the proton fluxes are anisotropic because of the bulk motion. It is found that an isotropic distribution, such as the Maxwell-Boltzmann or the K-distribution, transformed to a reference frame moving with the bulk velocity, provides a reasonable representation of these particle fluxes. Under these conditions, the particle phase space density distribution is found by transforming the isotropic distribution $f(\bar{w})$ to a coordinate system moving with a bulk velocity $\bar{V}_s$. Using the Liouville Theorem, in which the phase space density remains constant under the transformation,

$$f_1(\bar{w}) = f_2(\bar{v}-\bar{V}_s) \tag{A.14}$$

where

$$\bar{w} = \bar{v} - \bar{V}_s \tag{A.15}$$

and $\bar{w}$ is the thermal velocity, $\bar{v}$ is the observed particle velocity, $\bar{V}_s$ is the bulk velocity, and f_1 and f_2 are the phase space density distributions in the stationary and moving reference frames, respectively. Thus, referring to (A.1), a Maxwell-Boltzmann distribution moving with a bulk velocity $\bar{V}_s$ can be written

$$f_m = n \left(\frac{m}{2\pi kT}\right)^{3/2} \cdot e^{-\frac{m|\bar{v}-\bar{V}_s|^2}{2kT}} \tag{A.16}$$

and using (A.12), the flux is given by

$$j_m = \frac{n m^{1/2} v^2}{(2\pi kT)^{3/2}} \cdot e^{-\frac{m|\bar{v}-\bar{V}_s|^2}{2kT}} \tag{A.17}$$

where

$$|\bar{v}-\bar{V}_s|^2 = v^2 + V_s^2 - 2v\,V_s\cos\theta \qquad (A.18)$$

and θ is the angle between the observed particle velocity and the bulk velocity. In a similar manner, the K-distribution flux can be found for a moving reference frame by combining equations (A.2), (A.3), and (A.15) to obtain the new phase space density distribution function; then, using (A.12) to obtain the differential-energy unidirectional flux. The result gives

$$j_K = \frac{nK!\left(\frac{m}{2\pi}\right)^{3/2} v^2}{\Gamma(K-\frac{1}{2})\,(K-\frac{3}{2})^{3/2}(kT)^{3/2}} \cdot \frac{1}{\left[1 + \frac{m|\bar{v}-\bar{V}_s|^2}{2(K-\frac{3}{2})kT}\right]^{K+1}} \qquad (A.19)$$

where $|\bar{v}-\bar{V}_s|$ is as given by (A.18).

All calculations for this study have been made using the following values for the physical constants: proton mass (m_p) = 1.67×10^{-27} kg (1.04×10^{-12} eV•s•cm^{-2}); electron mass (m_e) = 9.11×10^{-31} kg (5.66×10^{-16} eV•s•cm^{-2}); Boltzmann constant (k) = 1.38×10^{-23} J•K^{-1} (8.625×10^{-5} eV•K^{-1}).

Appendix B. The Derivation of a Time-Averaged, Solar Wind Proton Spectrum

Typical solar wind fluxes, observed over a period of months, may show bulk speed variations of more than a factor of two. Using a Maxwell-Boltzmann distribution function in a reference frame moving with the bulk speed to represent Vela 3A and 3B data, *Gosling et al.* (1970) have made a statistical study of the relationships among various solar wind parameters. These observations, covering the time interval July 1965 to November 1967, were made near solar minimum and during a rising portion of the solar cycle. Based on an 11-year cycle, the next corresponding period (1976 to 1978) should overlap the ISEE-A/-B launch date. In any event, a strong solar-cycle dependence for the solar wind parameter relationships is not expected.

Table 3 presents the Vela 3A and 3B correlations between the solar wind velocity (V_S) and density (n) and temperature (T). Also given is the normalized frequency of occurrence (probability) of solar wind velocities in specified ranges. By combining these data with the expression for a Maxwell-Boltzmann distribution in the moving frame as given by equations (A.15) and (A.16) of Appendix A, it is possible to construct a time-averaged, solar wind proton spectrum ($\bar{j}_S$). Writing the solar wind proton spectrum (j_S) to show the explicit dependence of n and T on solar wind speed, yields

$$j_s\,(V_S) = \frac{n(V_S)\; m^{1/2}\; v^2}{[2\pi k T(V_S)]^{3/2}} \cdot e^{-\frac{m}{2kT(V_S)}(v^2 + V_s^2 - 2v\,V_s\cos\theta)} \qquad (B.1)$$

where parameters not defined here are as given in Appendix A. The time-averaged spectrum ($\bar{j}_S$) can now be obtained from

$$\bar{J}_s = \int_{V_{min}}^{V_{max}} j_s\,(V_S)\,\frac{dF}{dV_S}\,dV_S \qquad (B.2)$$

where

$$\int_{V_{min}}^{V_{max}} \frac{dF}{dV_S}\,dV_S = 1 \qquad (B.3)$$

F is defined as the probability that the bulk solar wind speed is V_S, and V_{min} and V_{max} are the minimum and maximum solar wind velocities presented in Table 3. The resulting spectrum, looking into the bulk flow ($\theta=0$), has a much broader energy spread than any individual observation

and is shown in Figure 4. The peak flux occurs near 600 eV and nearly all the flux lies between 300 and 2000 eV. A technique for obtaining a useful average spectrum from this highly anisotropic flux is given in Appendix C.

Appendix C. The Derivation of a Spin-Averaged, Solar Wind Proton Spectrum

The highly anisotropic solar wind proton flux can be reasonably approximated by a Maxwell-Boltzmann distribution in a reference frame moving with the bulk flow speed. From Appendix A, the differential energy spectrum (j_s) can be written as

$$j_s = \frac{nm^{3/2} v^2}{(2\pi kT)^{3/2}} \cdot e^{-\frac{m}{2kT}(v^2 + V_s^2 - 2vV_s \cos\eta)} \qquad (C.1)$$

where v is the observed particle velocity, V_s is the solar wind (bulk flow) velocity, θ is the angle between v and V_s, and kT is a characteristic thermal energy. The other parameters are as defined in Appendix A. Typical values for the bulk flow energy (E_f), given by

$$E_f = \tfrac{1}{2}mV_s^2 \qquad (C.2)$$

are two orders of magnitude larger than the characteristic thermal energy (kT). This anisotropic flux cannot easily be used for this study in the form given by equation (C.1). Since one objective of this study is to assess the radiation flux received by the spinning ISEE-A/-B spacecraft, it is appropriate to consider the specified geometry.

Figure 19 shows a schematic representation of a plane area (dA) as an approximation to the side of the spinning ISEE-A/-B spacecraft, where the spin axis is perpendicular to the ecliptic (X-Z) plane and to the bulk flow direction (V_s). The radiation received by this plane area will vary with the angle η as the spacecraft spins in the presence of an anisotropic flux like the solar wind. The approach adopted is to construct an effective isotropic flux (j_{se}) that will provide the same radiation through the plane area (dA) as the average received during one rotation. This effective isotropic flux may then be compared and combined with other isotropic fluxes, with the restriction that it only be used to determine the average radiation on a spinning plane area when the spin axis is perpendicular to the bulk flow.

As is well known, the flux through an area from one side (hereafter referred to as area flux, j_A) in the presence of an isotropic differential flux (j) is independent of orientation and is given by

$$j_A = \int j \, d\Omega = \pi j \qquad (C.3)$$

where $d\Omega$ is a differential solid angle, and typical units of j_Λ are [particles/($cm^2 \cdot s \cdot eV$)]. It is now necessary to calculate the spin-averaged area flux ($\bar{j}_\Lambda$) in the solar wind. Using equation (C.1) and referring to the geometry of Figure 19, j_Λ for a given angle η can be written as

$$j_A(\eta) = \int j_\Lambda(\theta) \cos \xi \, d\Omega \tag{C.4}$$

where

$$\cos \theta = \cos \xi \cos \eta + \sin \xi \sin \eta \cos \phi \tag{C.5}$$

$$d\Omega = \sin \xi \, d\xi \, d\phi \tag{C.6}$$

The spin-averaged area flux (j_A) is now found by averaging over the angle η to give

$$\bar{j}_A = \frac{1}{\pi} \int_0^\pi j_A(\eta) \, d\eta \tag{C.7}$$

where, by symmetry, the integration need only be carried out over a half rotation.

In general, combining equations (C.4) and (C.7) requires a triple numerical integration. However, an approximation is possible in this case since the thermal component of particle energy is a small fraction of the bulk flow component. Rewriting equation (C.4) with $\eta = 0$, gives

$$j_A(0) = \int_{\xi=0}^{\pi/2} \int_{\phi=0}^{2\pi} \frac{n m^{1/2} v^2}{(2\pi kT)^{3/2}} \cdot e^{-\frac{m}{2kT}(v^2 + V_s^2 - 2vV_s \cos \xi)} \cdot \cos \xi \sin \xi \, d\xi \, d\phi \tag{C.8}$$

where $\theta = \xi$ from equation (C.5). Performing these integrations yields

$$j_A(0) = \frac{n(kT)^{1/2}}{(2\pi m)^{1/2} m V_S^2} \left[\left(\frac{mvV_S}{kT} - 1 \right) e^{-\frac{m}{2kT}(v - V_s)^2} + e^{-\frac{m}{2kT}(v^2 + V_s^2)} \right] \tag{C.9}$$

where $j_\Lambda(o)$ is the area flux for a unit area that is perpendicular to the bulk flow. By making the approximation that this flow has no thermal component, the area flux at angle η is given by

$$j_A(\eta) \approx j_A(0) \cos \eta \qquad (C.10)$$

for $|\eta| \leq \pi/2$ and zero elsewhere. Substituting $j_A(\eta)$ into equation (C.7) yields

$$\bar{j}_A(\eta) \approx \frac{1}{\pi} \int_0^{\pi} j_A(\zeta) \cos \eta \, d\eta \approx \frac{j_A(0)}{\pi} \qquad (C.11)$$

for the spin-averaged area flux. This approximate expression is accurate to better than 1 percent as indicated by computing the triple numerical integration implicit in equations (C.4) and (C.7) for the solar wind parameters given in Table 3. Therefore, the effective isotropic flux (j_{se}), using equations (C.3) and (C.11), can be expressed as

$$j_{se} = \frac{j_A(0)}{\pi^2} \qquad (C.12)$$

where $j_A(o)$ is given in (C.9). Time averaging of $j_A(o)$ has been performed using the procedure given in Appendix B. The resulting time- and spin-averaged effective isotropic flux is shown in Figure 4.

Other geometries, besides that given in Figure 19, may be useful in some cases. One of these is the radiation received by a sphere of unit cross section, which requires a determination of the omnidirectional flux (j_o). For the solar wind, j_o is given by

$$j_o = \int j_s(\theta) \, d\Omega \qquad (C.13)$$

where $j_s(\theta)$ is given by equation (C.1), and $d\Omega$ is given by equation (C.6) with $\theta = \zeta$. The result gives

$$j_o = \frac{2\pi kT}{mvV_s} \left[j_s(\theta=0) - j_s(\theta=\pi) \right] \qquad (C.14)$$

where typical units of j_o are [particles/($cm^2 \cdot s \cdot eV$)]. This spectrum may also be time averaged using the procedure in Appendix B.

Appendix D. The Derivation of a Spin-Averaged, Magnetosheath Proton Spectrum Using a K-Distribution Function

The anisotropic magnetosheath proton flux can be reasonably approximated by an isotropic distribution function in a reference frame moving with a bulk flow speed. The K-distribution function, with K = 2, has been found to be appropriate in many cases (*Formisano et al.*, 1973) and also approximates the composite spectra shown in Figure 7. From Appendix A, the differential energy spectrum (j_K) with K = 2 can be written as

$$j_{K2} = \frac{4nm^{1/2}\, v^2}{\pi^2 (kT)^{3/2}} \cdot \frac{1}{\left[1 + \frac{m}{kT}\,(v^2 + V_f{}^2 - 2v\, V_f \cos\theta)\right]^3} \qquad (D.1)$$

where v is the observed particle velocity, V_f is the bulk flow velocity, θ is the angle between v and V_f, and kT is a characteristic thermal energy. The other parameters are as defined in Appendix A. Unlike the situation in the solar wind, the bulk flow energy (E_f) given by

$$E_f = \tfrac{1}{2} m V_f{}^2 \qquad (D.2)$$

is of the same order as the characteristic thermal energy (kT). Nevertheless, the anisotropy is generally sufficiently large that it is necessary to calculate an effective isotropic magnetosheath proton flux (j_{Ke}) as was done for the solar wind protons. This flux will provide the same radiation through a plane unit area as the average received by a spinning unit area with its spin axis perpendicular to the bulk flow velocity. If the spin axis is not perpendicular to the bulk flow velocity, this approach will overestimate j_{Ke}. A detailed description of the geometry is given in Appendix C and is shown in Figure 19.

The flux through the unit area (area flux $-j_A$) for arbitrary angle η can be written as

$$j_A(\eta) = \int j_{K2}(\theta) \cos\xi \, d\Omega \qquad (D.3)$$

where

$$\cos\theta = \cos\xi \cos\eta + \sin\xi \sin\eta \cos\phi \qquad (D.4)$$

$$d\Omega = \sin \xi \, d\xi \, d\phi \tag{D.5}$$

and $j_{K2}(\theta)$ is as given by equation (D.1). The spin-averaged area flux is now found by averaging over the angle η to give

$$\bar{j}_A = \frac{1}{\pi} \int_0^{\pi} j_A(\eta) \, d\eta \tag{D.6}$$

where, by symmetry, the integration need only be carried out over a half rotation. Using equation (C.3) from Appendix C, the effective isotropic flux can now be written as

$$j_{Ke} = \frac{\bar{j}_A}{\pi} \tag{D.7}$$

where the calculation of j_A involves a triple numerical integration.

The high- and low-estimate magnetosheath spectra of Figure 7 correspond to $j_{K2}(\theta=0)$ with V_f = 280 km/s and kT = 400 eV. These spectra differ only in the density parameter with n = 17 cm^{-3} and 2 cm^{-3} for the high and low estimates, respectively. The derived effective isotropic spectra (j_{Ke}) are also shown in that figure.

As discussed in Appendix C, flux estimates for other geometries may sometimes be useful. In particular, the omnidirectional flux (j_o) from a K-distribution, with K = 2, may be readily found from the expression

$$j_o = \int j_{K2}(\theta) \, d\Omega. \tag{D.8}$$

where $j_{K2}(\theta)$ is given by equation (D.1), and $d\Omega$ is given by equation (D.5) with $\theta = \xi$. The result can be written as

$$j_o = \frac{\pi kT}{2mvV_f} \left(j_{K2}(\theta=0) \cdot \left[1 + \frac{m}{kT}(v-V_f)^2\right] - j_{K2}(\theta=\pi) \cdot \left[1 + \frac{m}{kT}(v+V_f)^2\right] \right) \tag{D.9}$$

where typical units of j_o are [particles/($cm^2 \cdot s \cdot eV$)].

Table 1. Spatial Regions of the Near-Earth Environment for High-Altitude Satellites

Eight Regions (*Vette et al.*, 1976)	Five Regions (Present Study)
1. interplanetary medium	1. interplanetary medium
2. dayside magnetosheath	2. magnetosheath
3. nightside magnetosheath	
4. dayside magnetosphere	3. inner magnetosphere
5. nightside magnetosphere ($-10R_E<X_{GSE}<0$)	
6. midlatitude magnetotail ($X_{GSM}<-10R_E$, $2R_E<\lvert Z_{GSM}-Z_{neutral\ sheet}\rvert\leq 6R_E$)	4. plasma sheet
7. neutral sheet region ($X_{GSM}<-10R_E$, $\lvert Z_{GSM}-Z_{neutral\ sheet}\rvert\leq 2R_E$)	
8. high-latitude magnetotail ($X_{GSM}<-10R_E$, $\lvert Z_{GSM}-Z_{neutral\ sheet}\rvert>6R_E$)	5. high-latitude magnetotail

Table 2. ISEE-A/-B Orbit-Averaged Spectra

Energy (eV)	Je Differential Flux [electrons/(cm^2•s•sr•eV)]	Jap* Effective Differential Flux [protons/(cm^2•s•sr•eV)]
1×10^2	1.6×10^6	1.2×10^4
4×10^2	2.0×10^5	4.2×10^4
6×10^2	1.2×10^5	4.7×10^4
1×10^3	6.8×10^4	2.7×10^4
4×10^3	9.0×10^3	1.8×10^3
1×10^4	1.3×10^3	4.7×10^2
4×10^4	7.0×10^1	1.7×10^2
1×10^5	1.1×10^0	8.5×10^1

Energy (eV)	Jae Integral Area Flux** [electrons/(cm^2•s)]	Jap* Effective Integral Area Flux** [protons/(cm^2•s)]
1×10^2	1.1×10^9	2.25×10^8
4×10^2	5.6×10^8	2.0×10^8
1×10^3	3.4×10^8	1.2×10^8
4×10^3	1.0×10^8	6.2×10^7
1×10^4	3.5×10^7	4.8×10^7
4×10^4	5.0×10^6	2.3×10^7
8×10^4	1.7×10^6	6.0×10^6
1×10^5	0	0

*The proton fluxes have been spin averaged (see text) in such a way that they will give the average flux passing through a spinning area when the spin axis is perpendicular to the ecliptic plane.

**Note:

$$J_{A_i} \equiv \int_{E}^{10^5 eV} \pi J_i \, dE$$

Table 3. Proton Solar Wind Parameter Relationships*

Vs Velocity Interval (km/s)	dF Frequency In Interval	n Density (cm^{-3})	T Temperature (K)
250 - 300	.050	9.2	2.50×10^4
300 - 350	.245	8.5	4.50×10^4
350 - 400	.270	7.8	7.50×10^4
400 - 450	.190	7.5	1.12×10^5
450 - 500	.110	6.9	1.45×10^5
500 - 550	.065	6.5	1.75×10^5
550 - 600	.040	6.0	2.05×10^5
600 - 650	.020	5.8	2.20×10^5
650 - 700	.010	5.5	2.45×10^5

*Vela 3 - July 1965 to November 1967 (*Hundhausen et al.*, 1970).

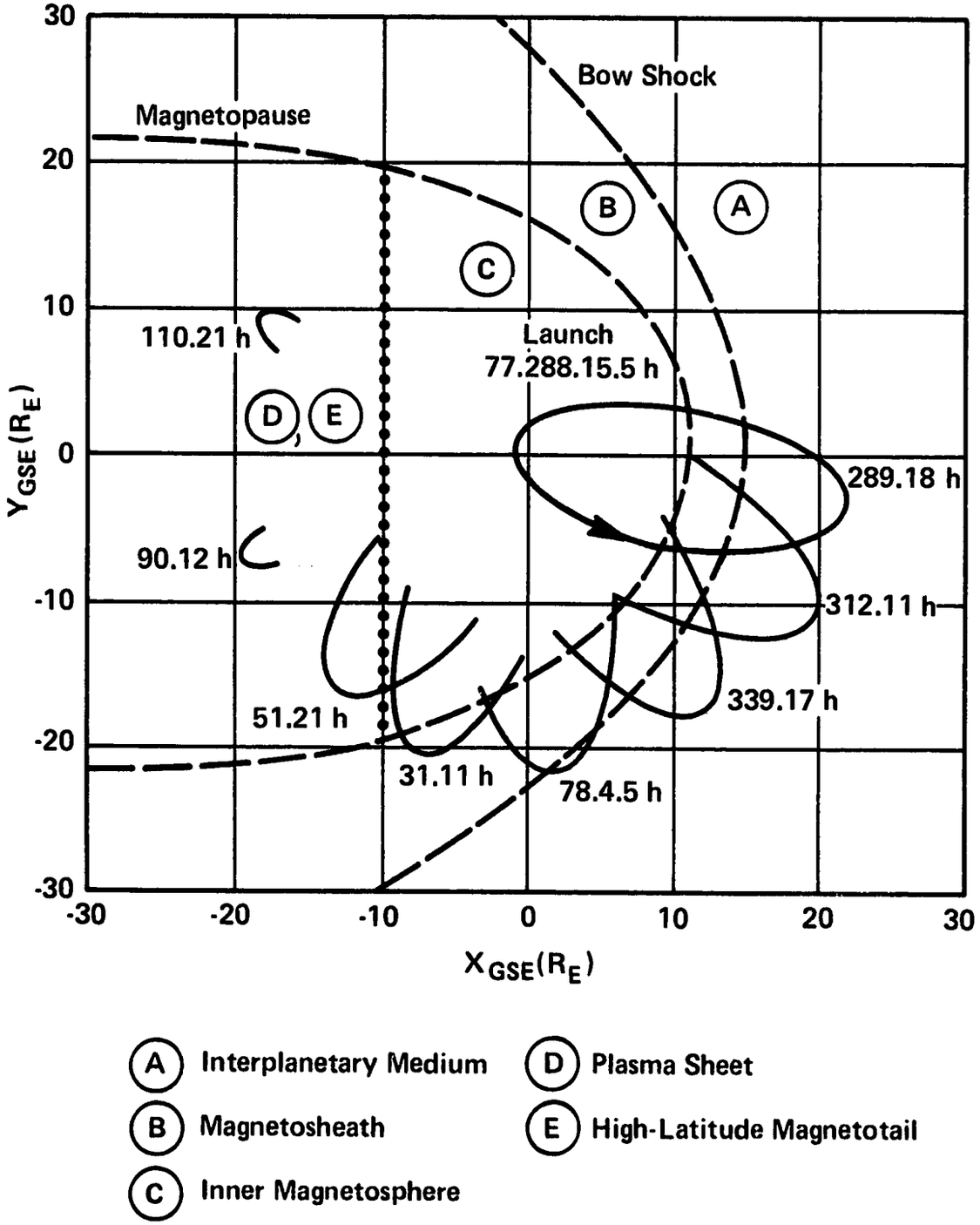

Figure 1. ISEE-A/-B Orbit Rotated into the GSE X-Y Plane

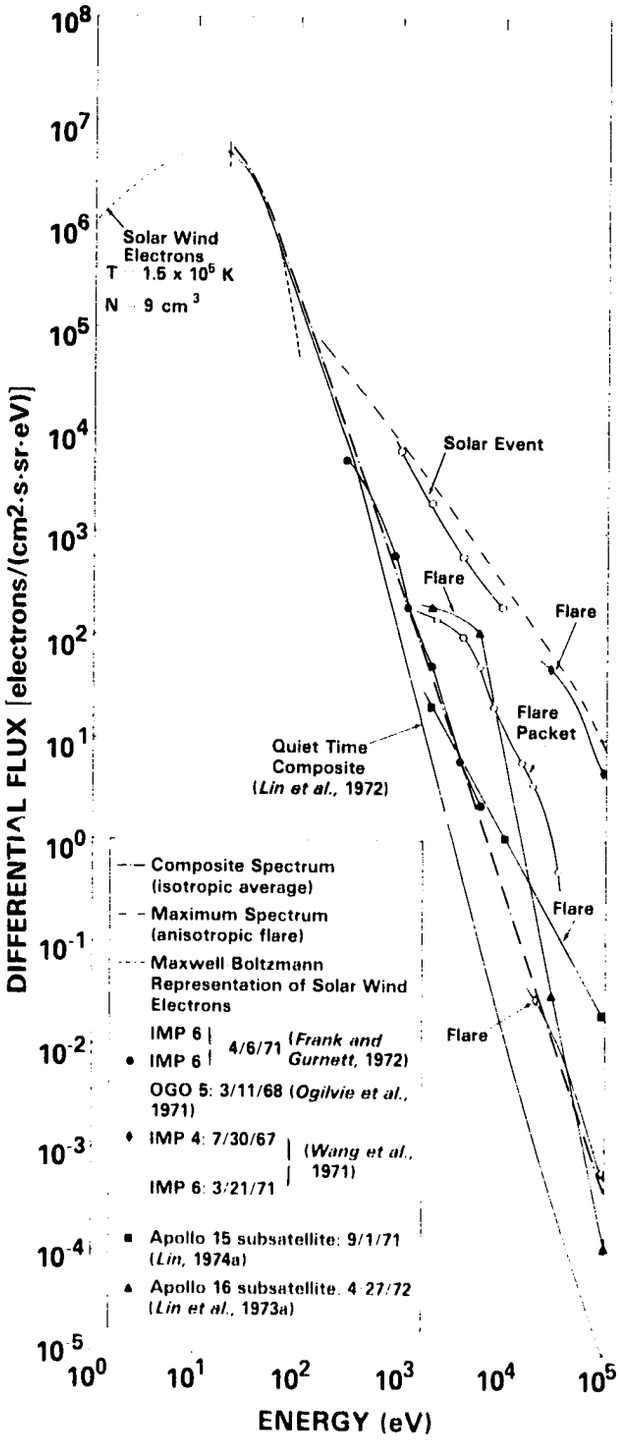

Figure 2. Interplanetary Electron Spectra

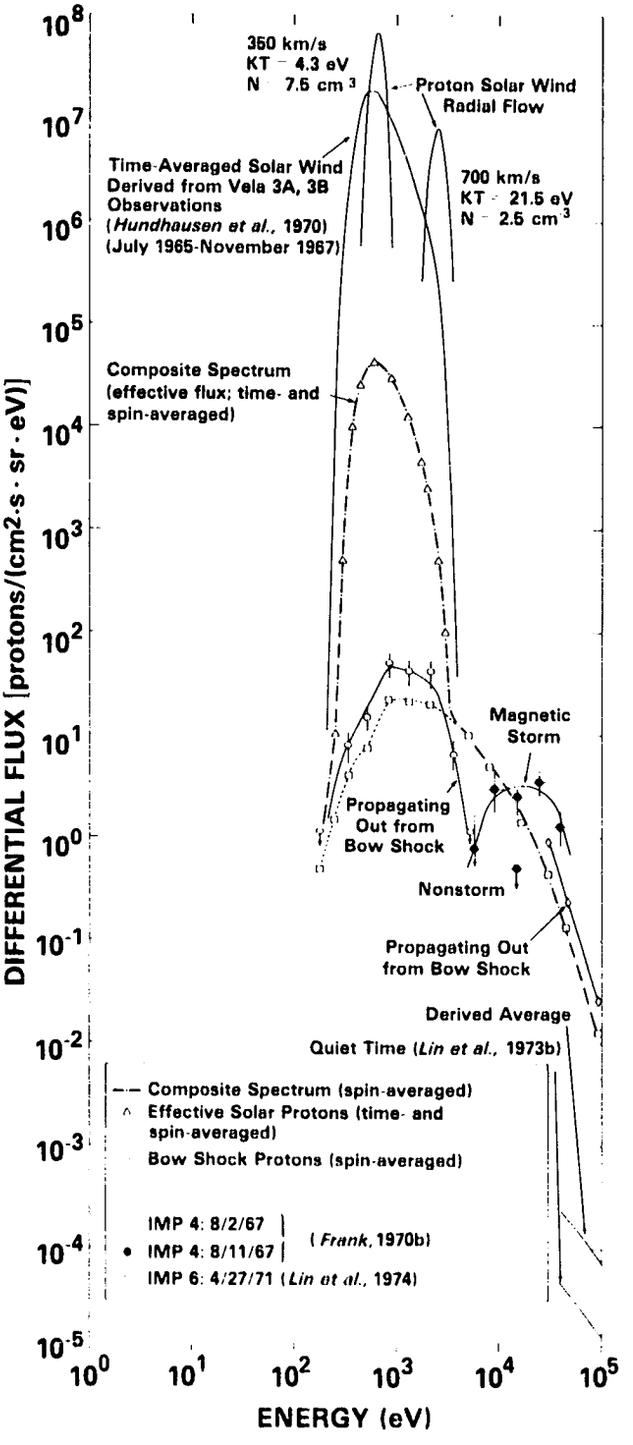

Figure 3. Interplanetary Proton Spectra

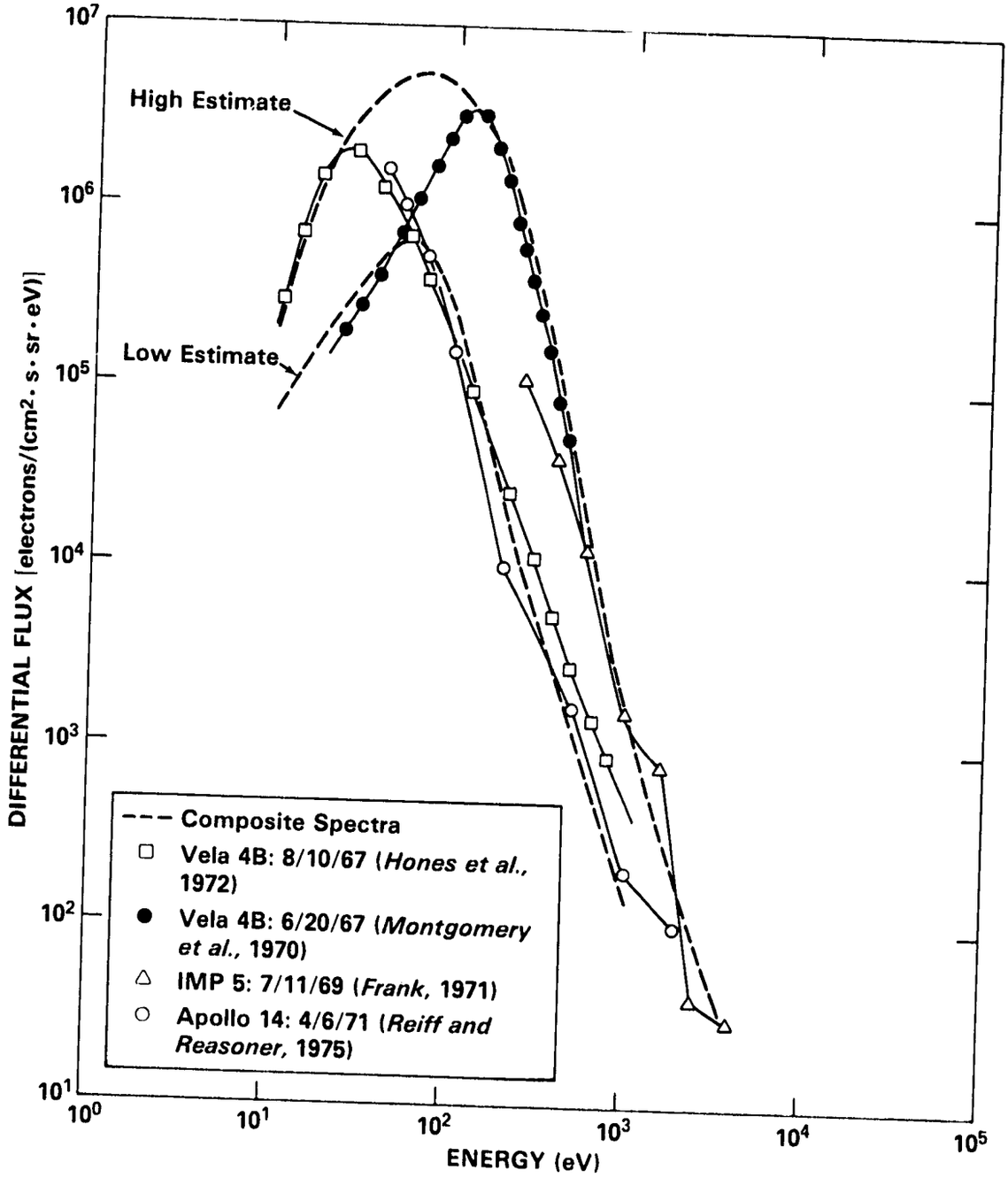

Figure 4. Magnetosheath Electron Spectra

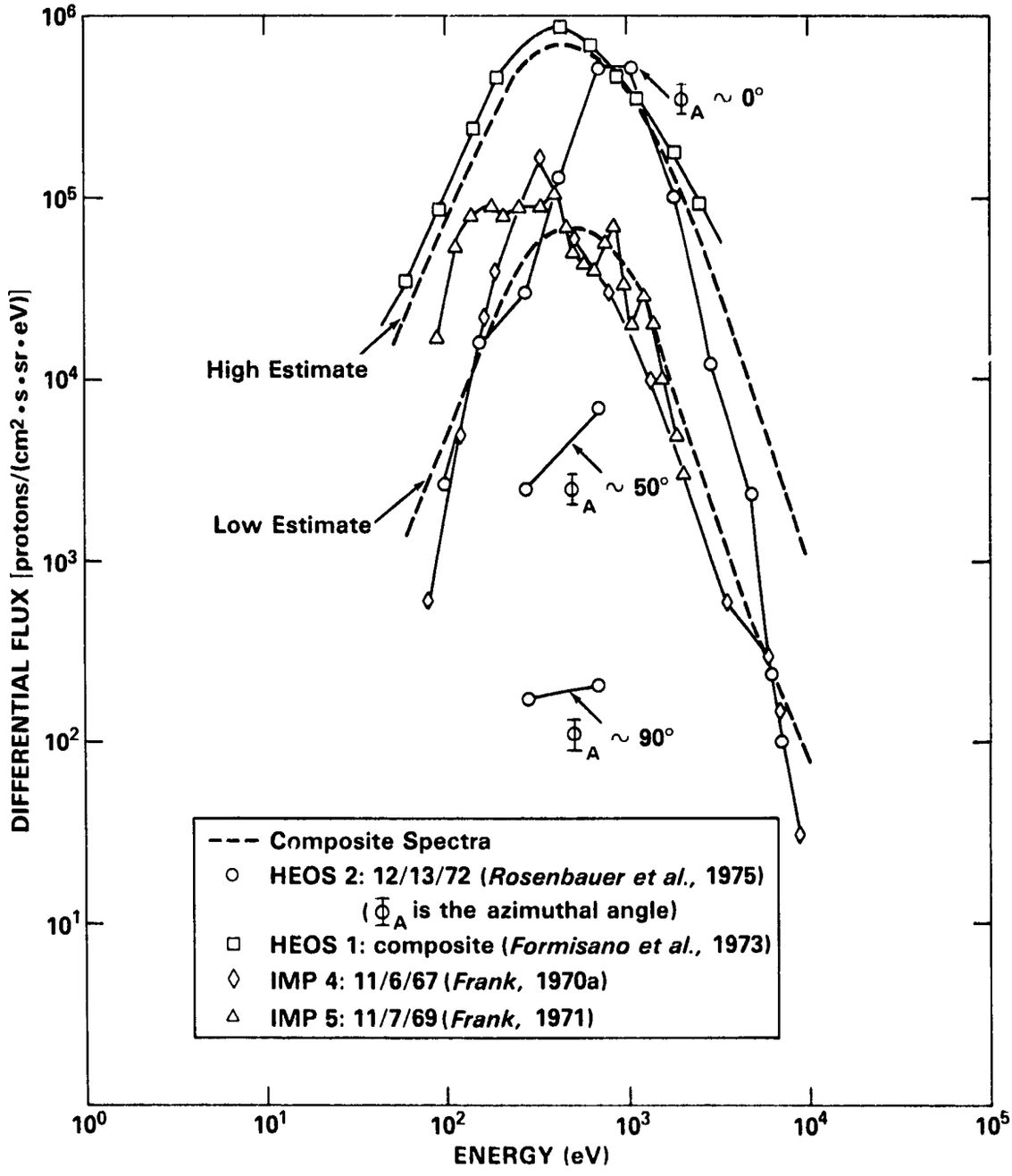

Figure 5. Magnetosheath Proton Spectra

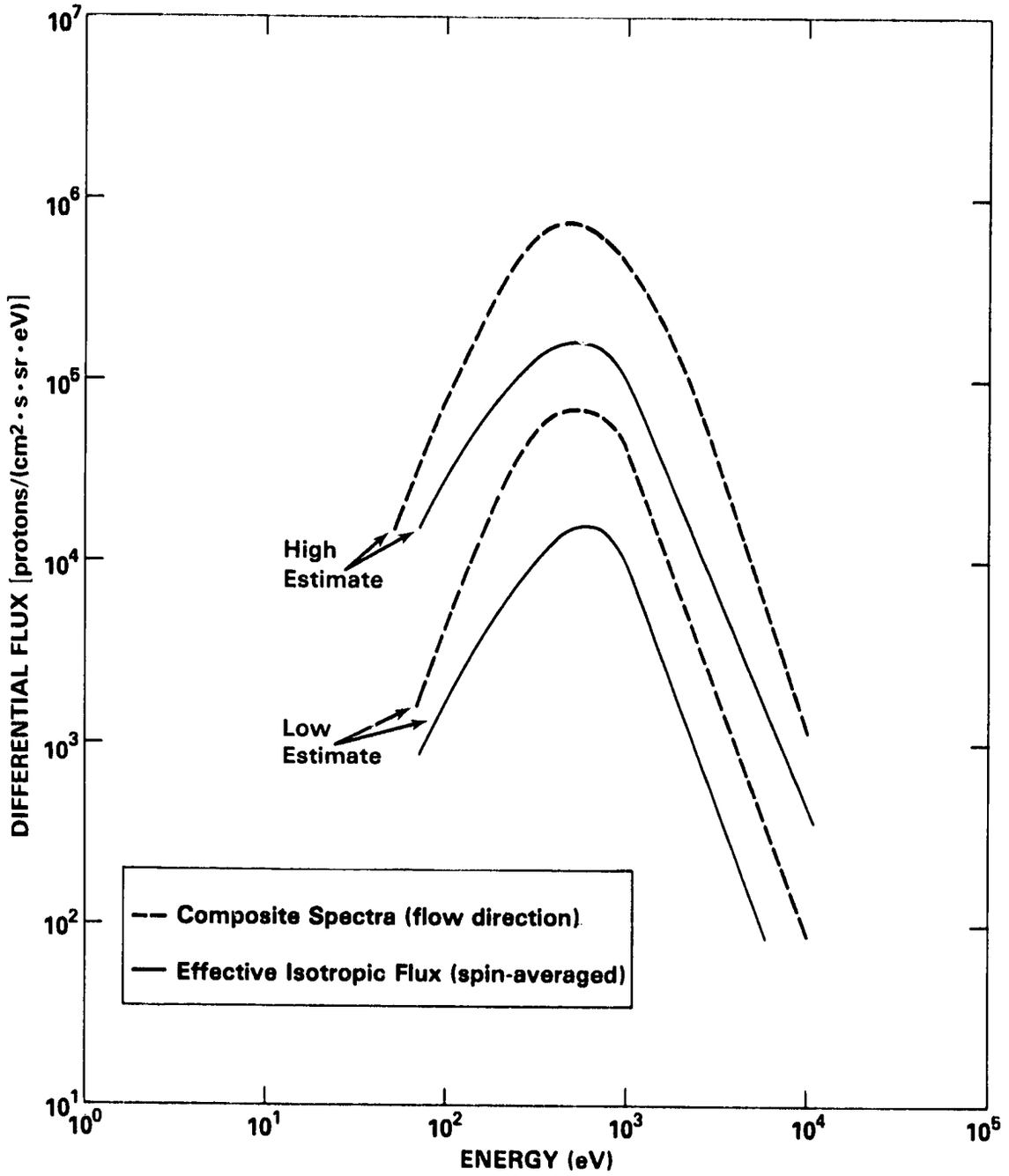

Figure 6. Magnetosheath Proton Spectra Compared with Spin-Averaged Spectra

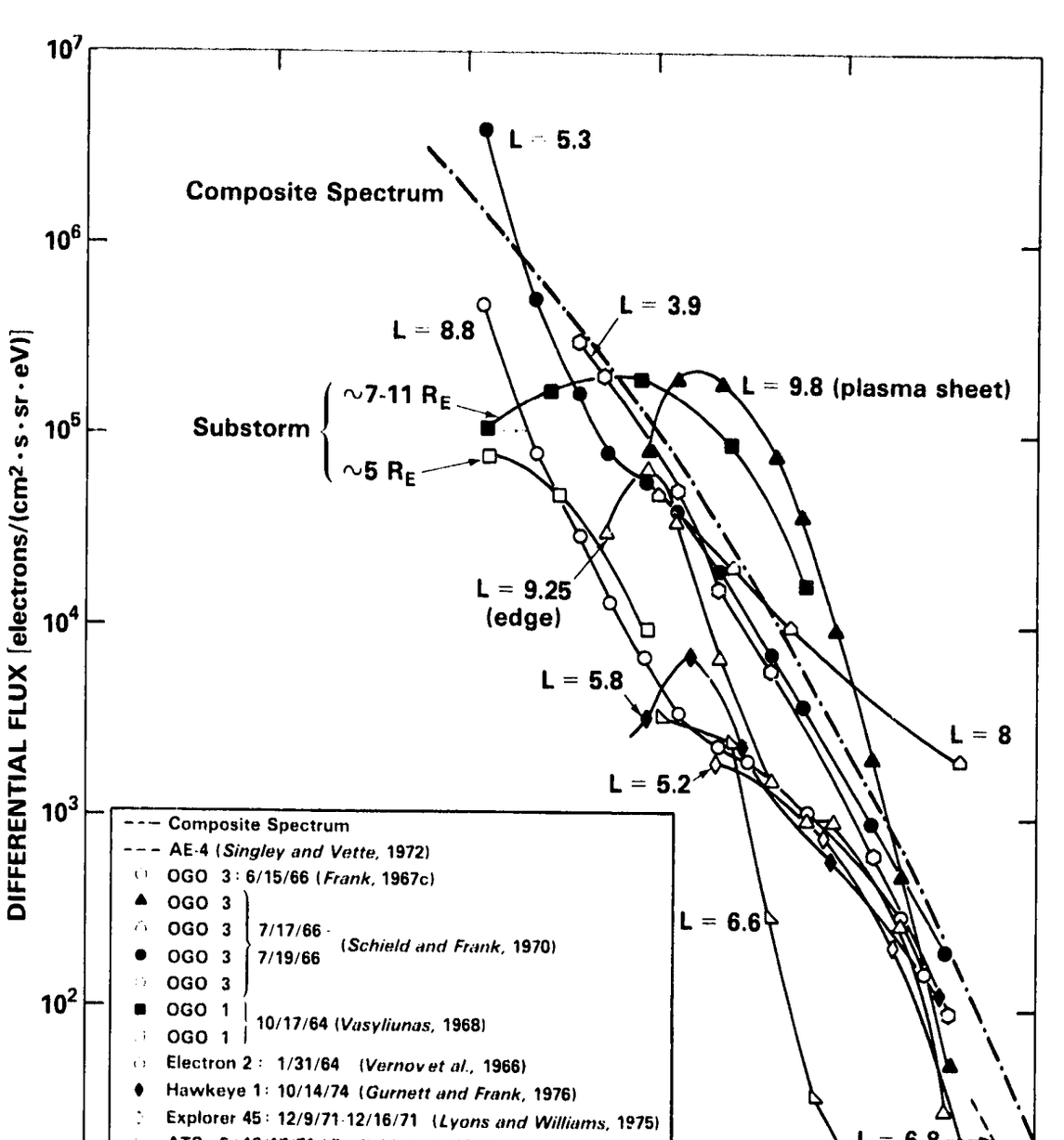

Figure 7. Inner Magnetosphere Electron Spectra

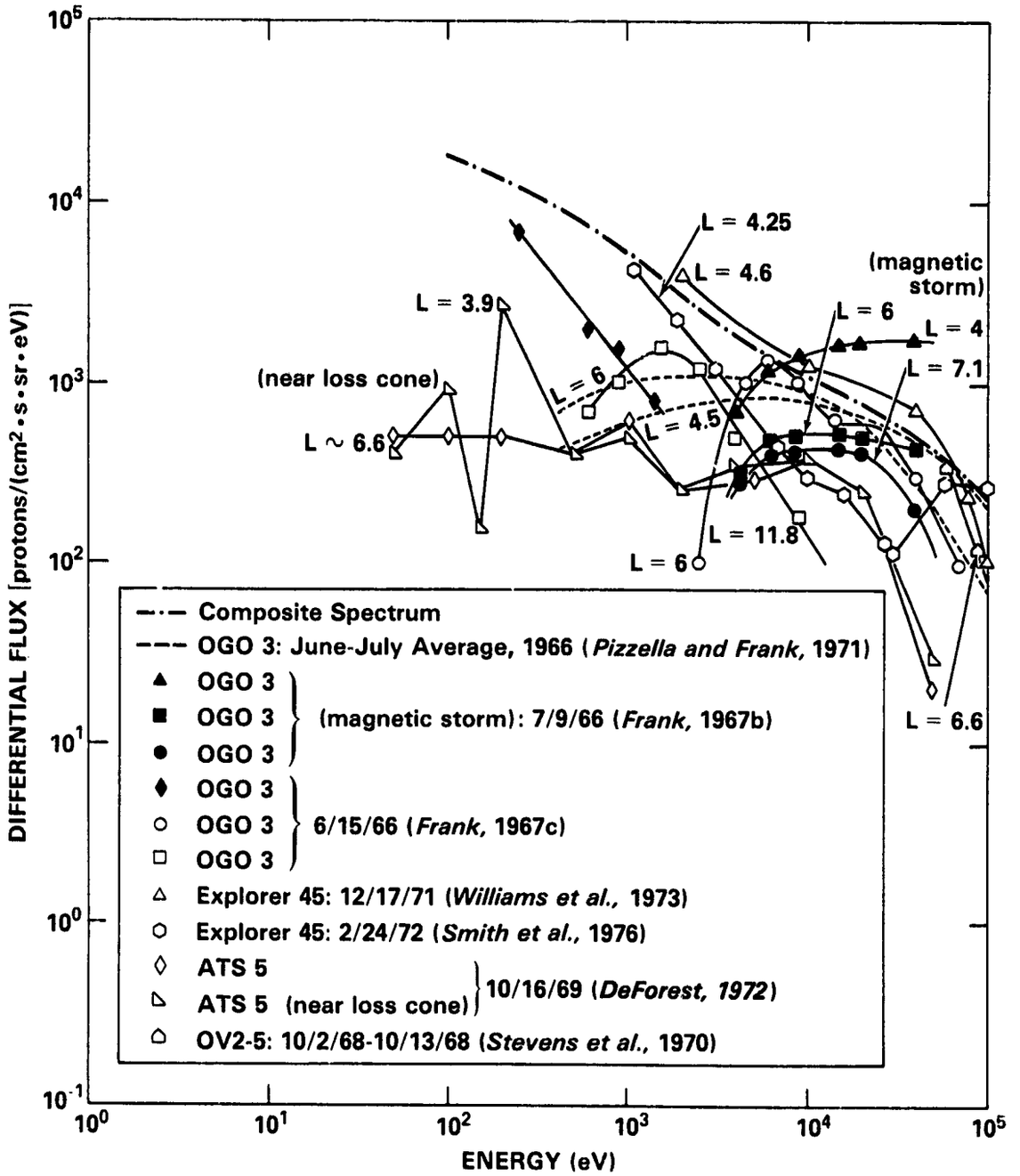

Figure 8. Inner Magnetosphere Proton Spectra

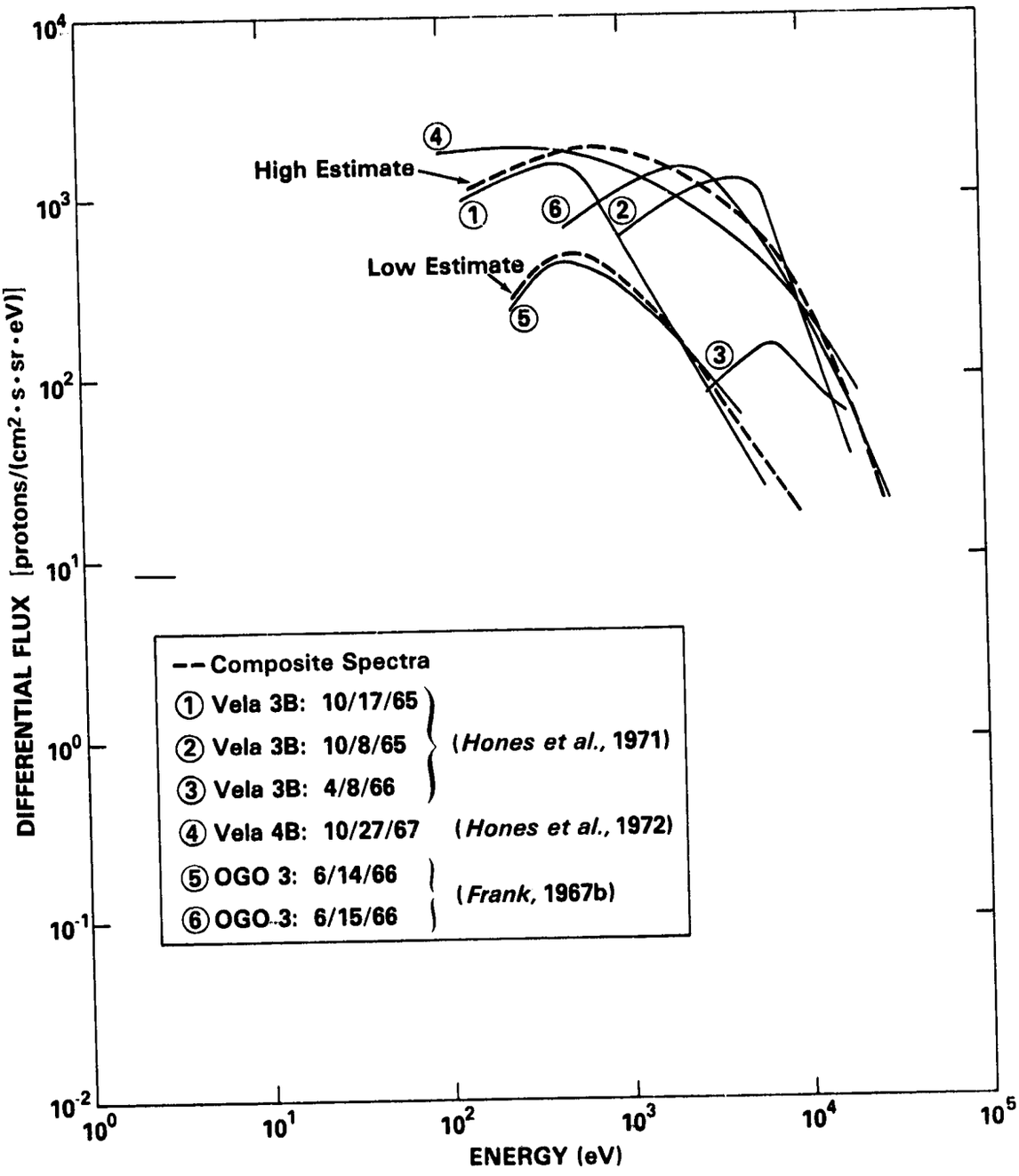

Figure 9. Plasma Sheet Proton Spectra

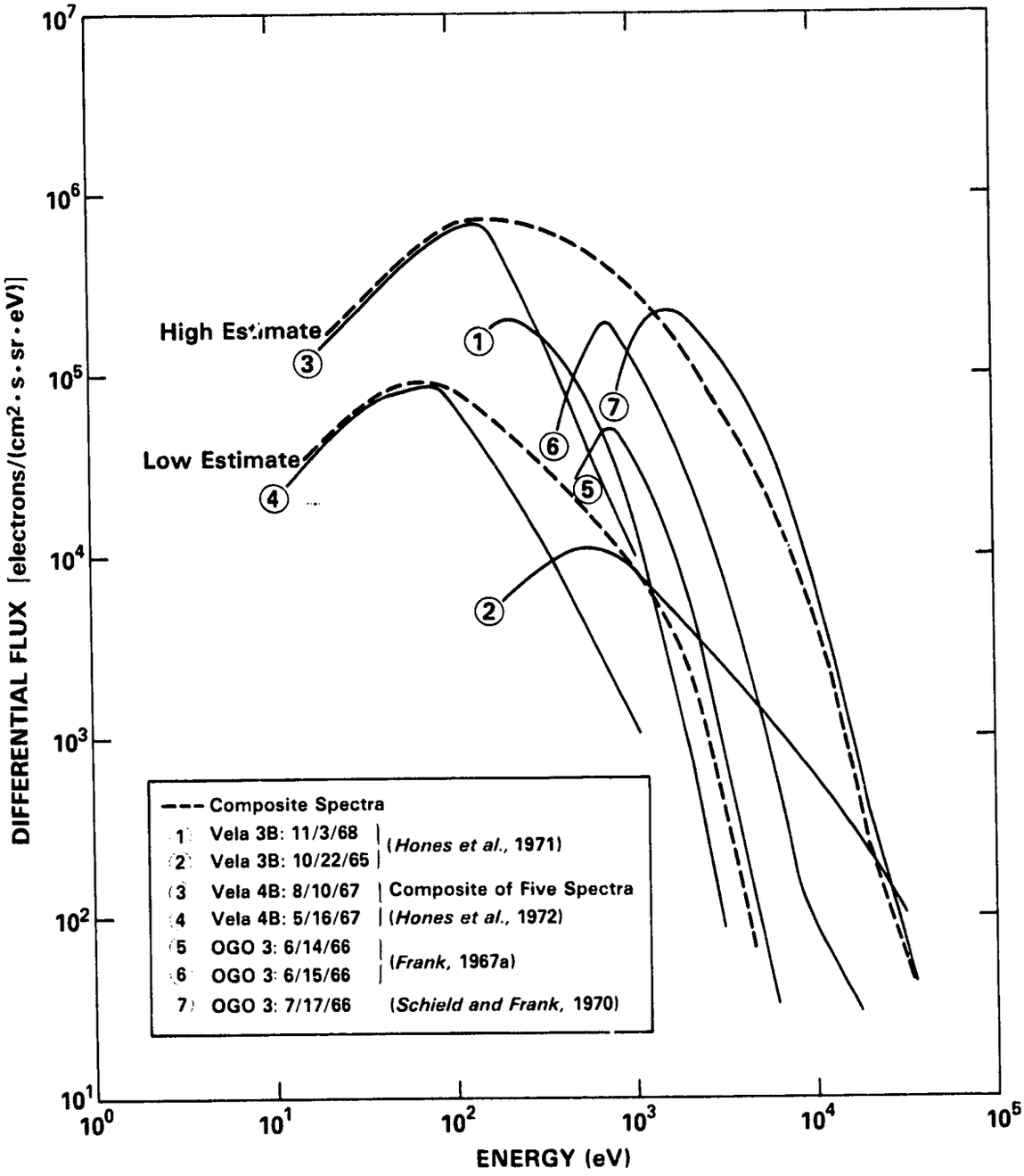

Figure 10. Plasma Sheet Electron Spectra

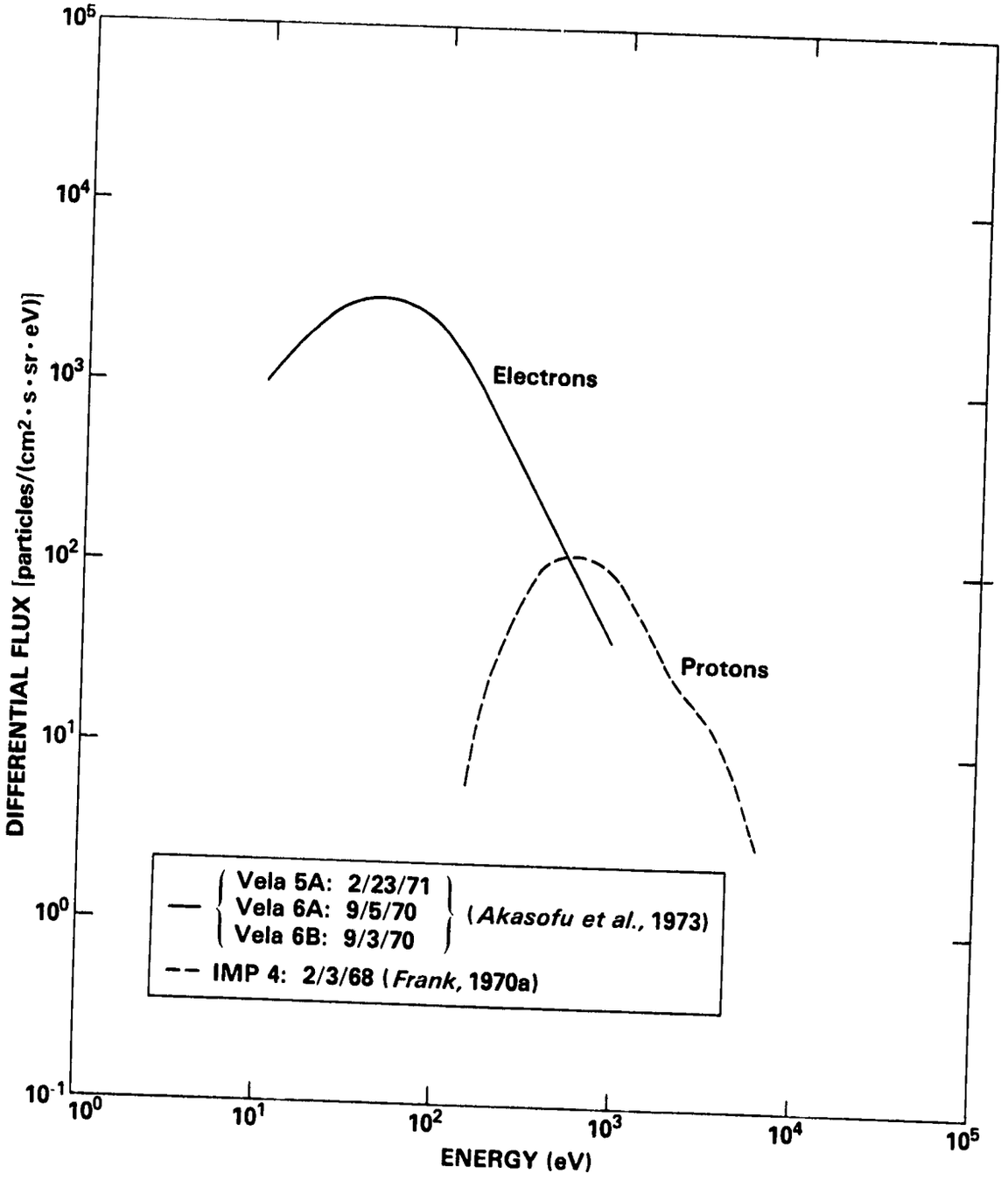

Figure 11. High-Latitude Magnetotail Spectra

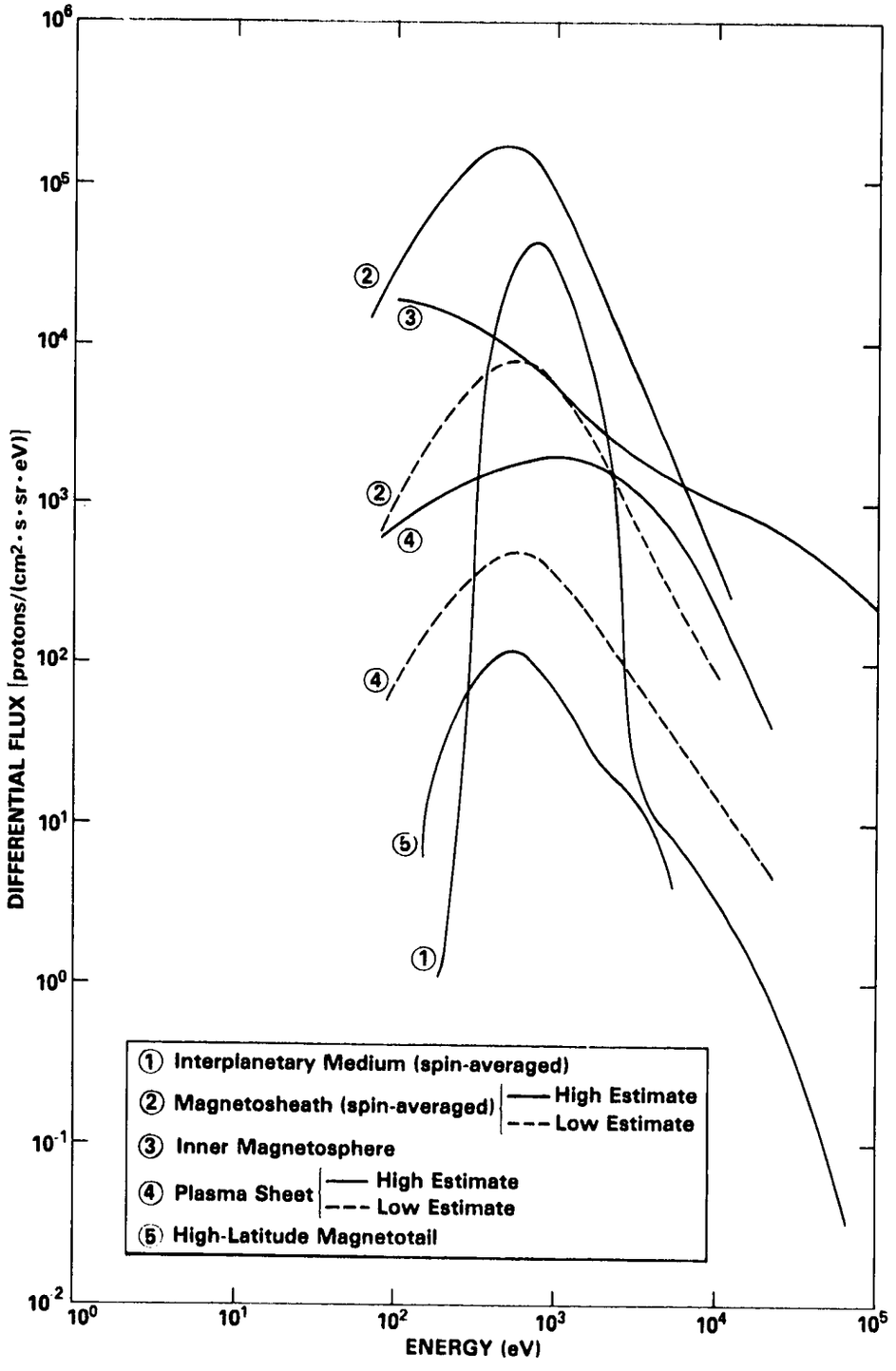

Figure 12. Composite Proton Spectra

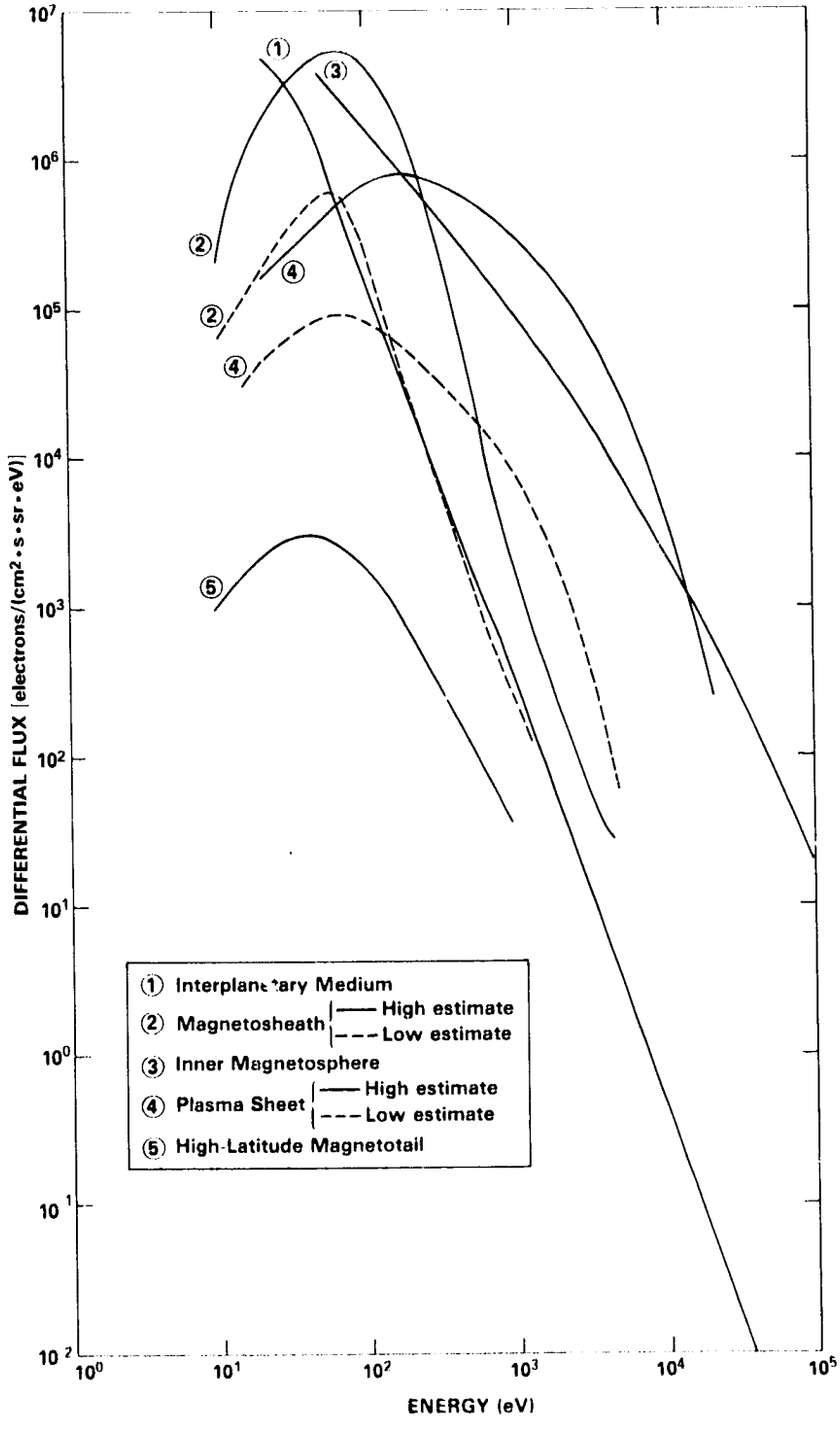

Figure 13. Composite Electron Spectra

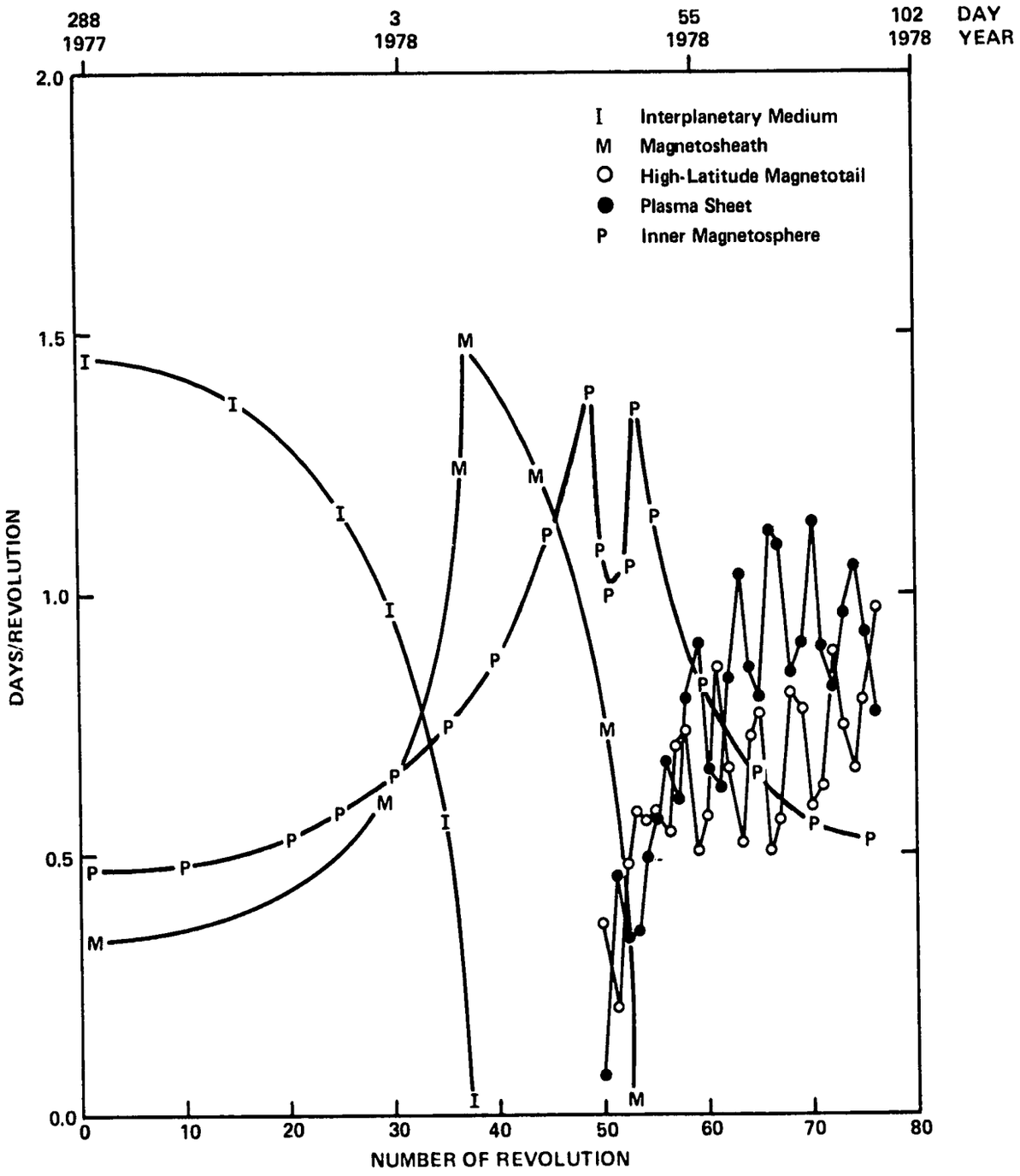

Figure 14. ISEE-A/-B Orbital Coverage (period ~ 2.3 days)

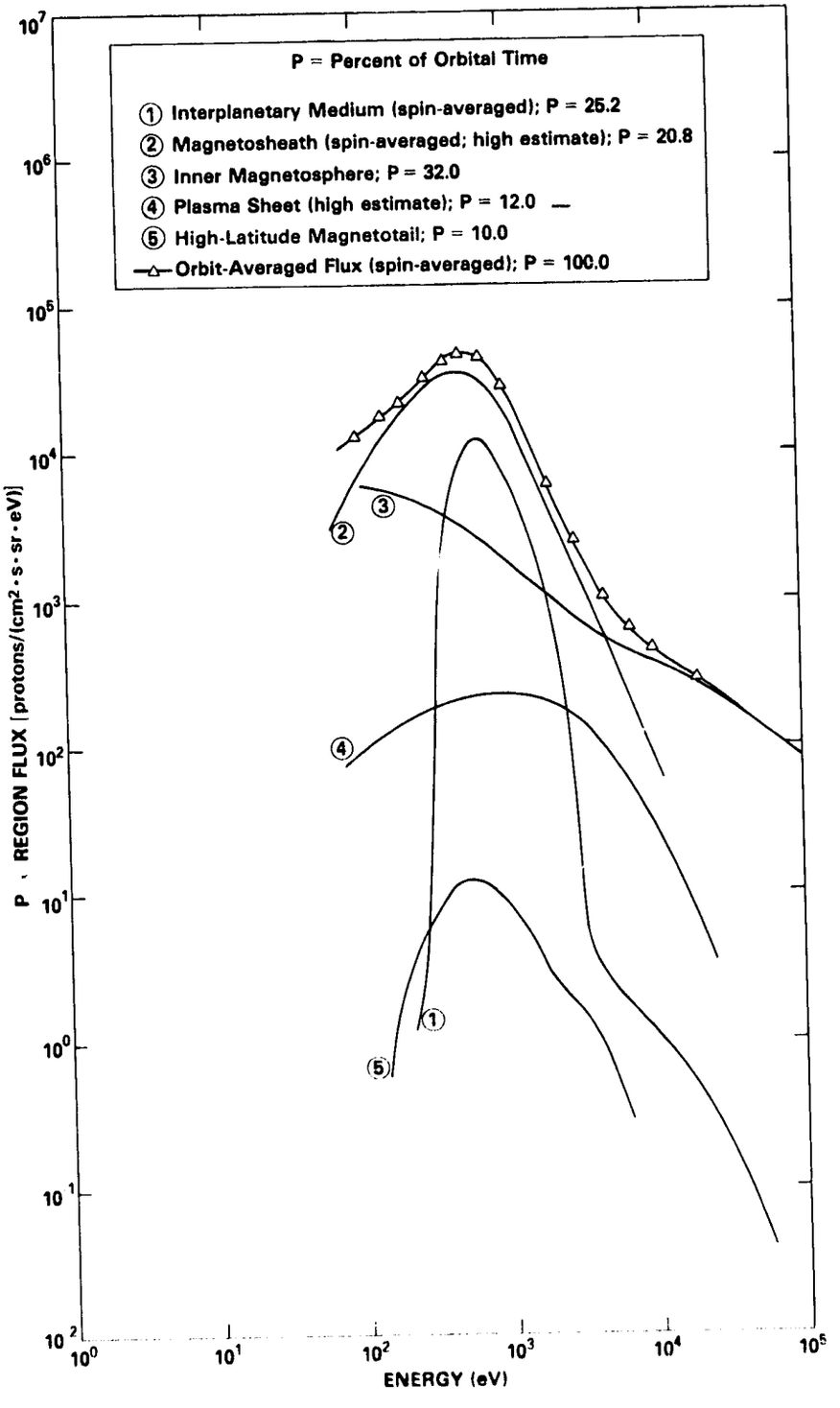

Figure 15. ISEE-A/-B Orbit-Averaged Proton Spectra (revolutions 1-76)

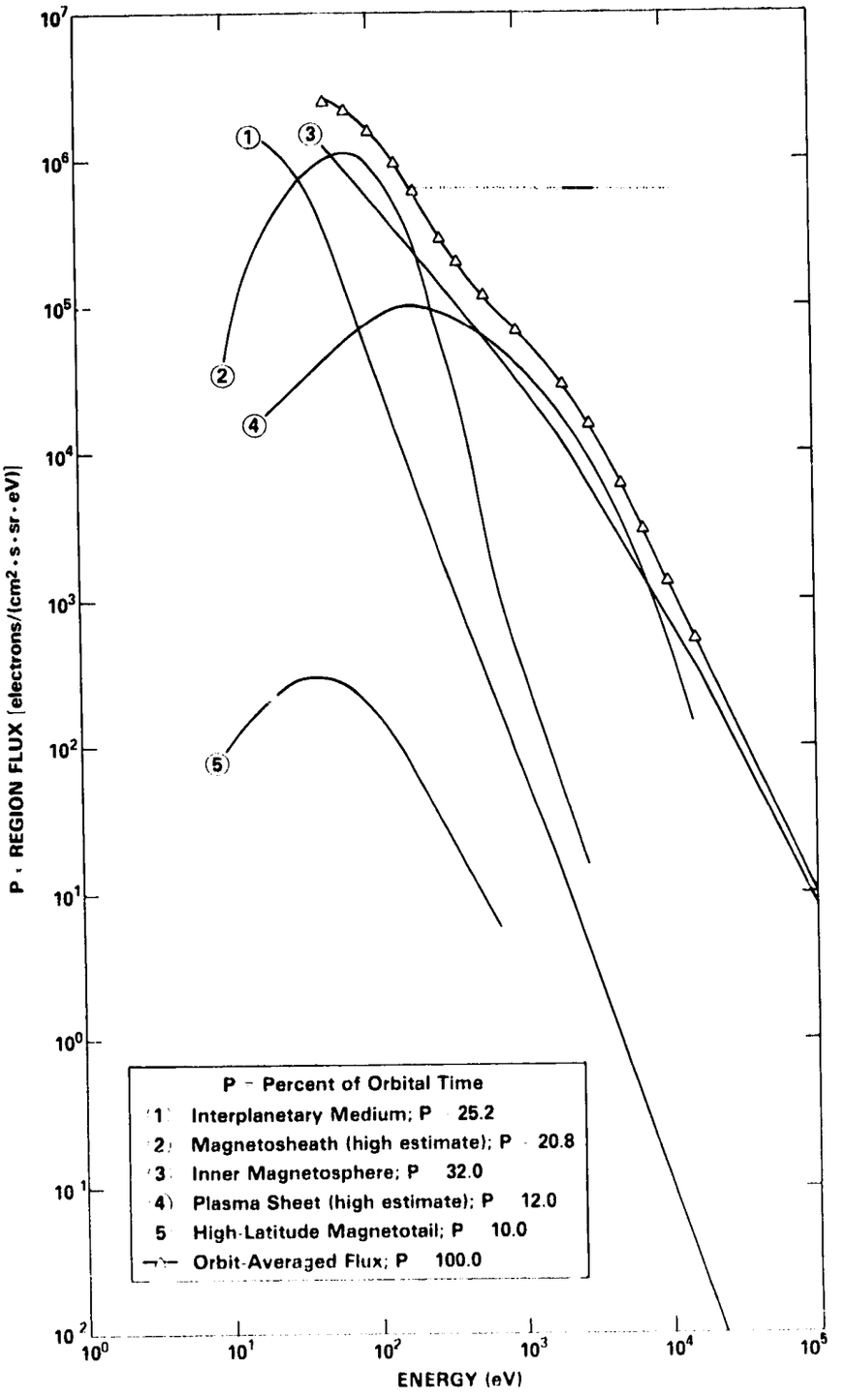

Figure 16. ISEE-A/-B Orbit-Averaged Electron Spectra (revolutions 1-76)

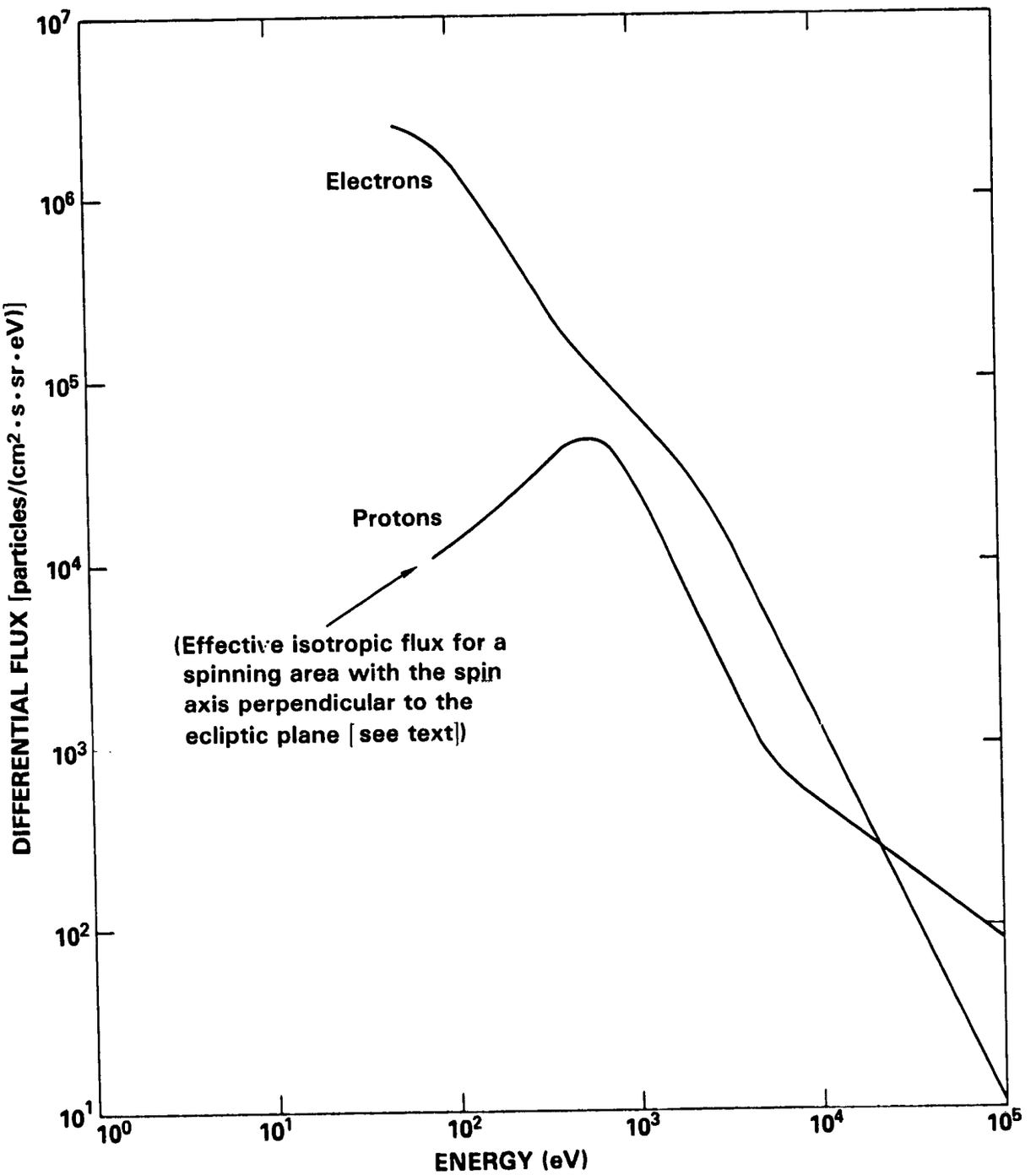

Figure 17. ISEE-A/-B Orbit-Averaged Differential Spectra (revolutions 1-76)

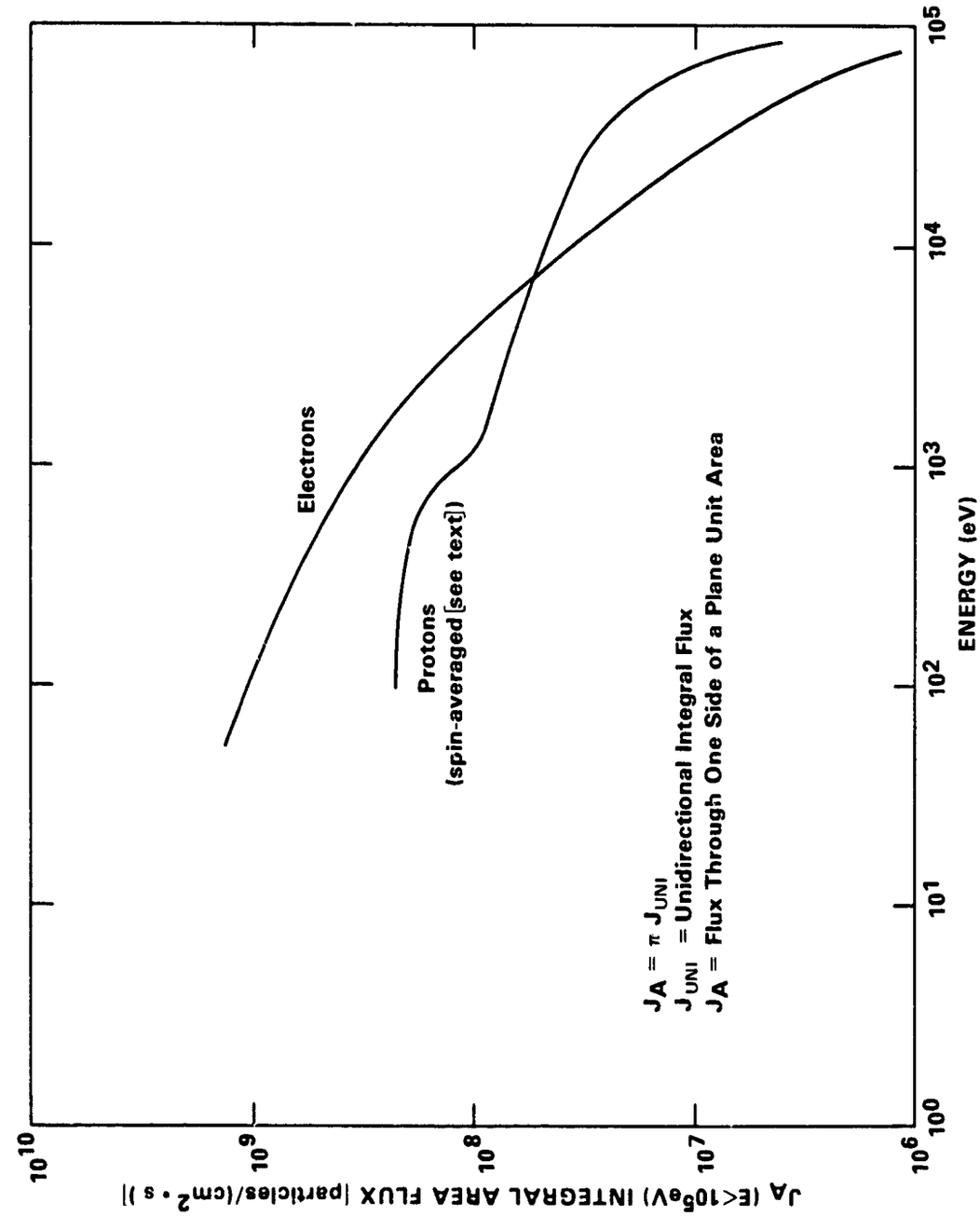

Figure 18. ISEE-A/-B Orbit-Averaged Integral Spectra for E < 10^5 eV (revolutions 1-76)

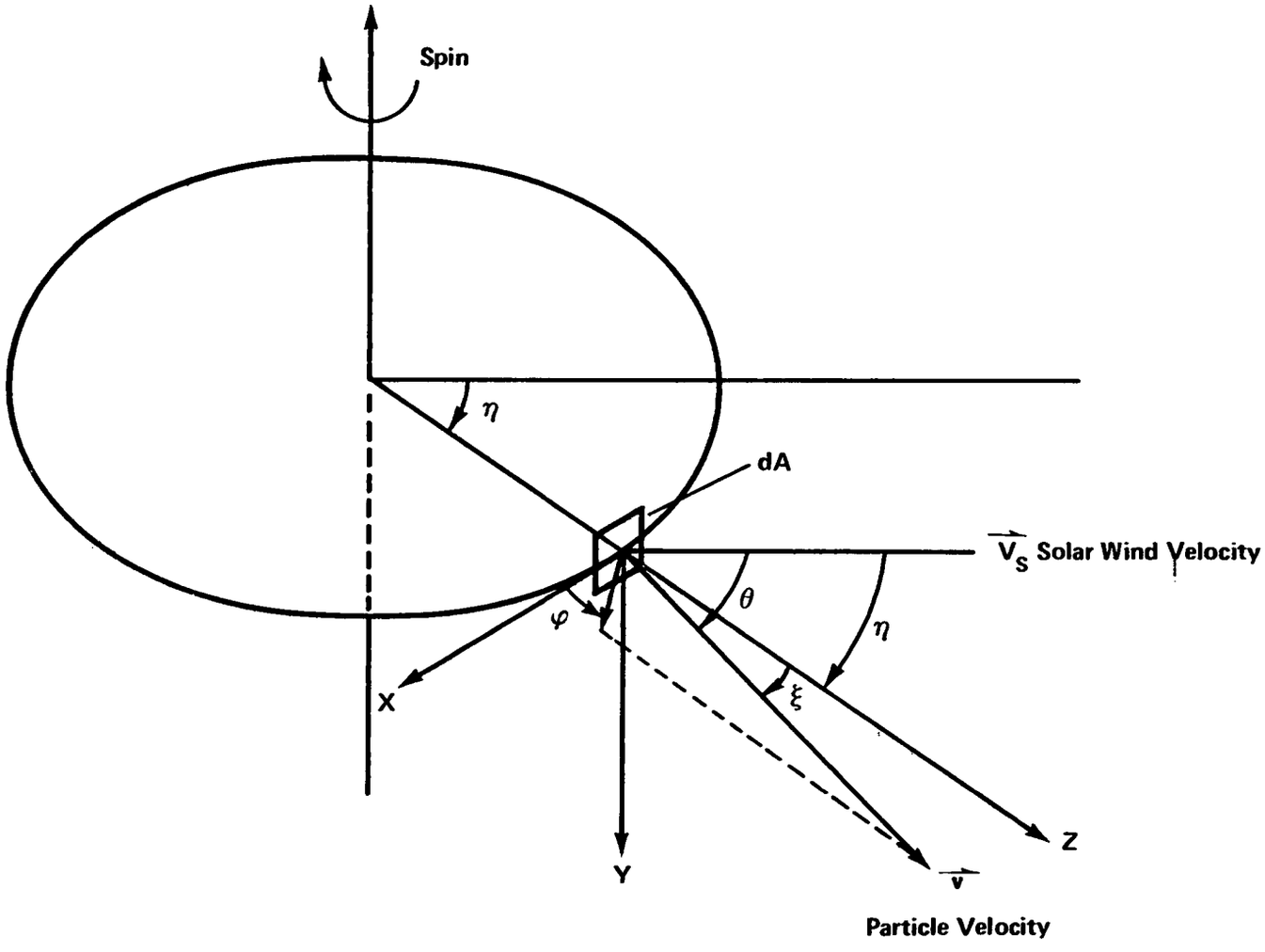

Figure 19. Spin-Averaging Geometry for Area Flux Computations

REFERENCES

Akasofu, S.-I., E.W. Hones, Jr., S.J. Bame, J.R. Asbridge, and A.T.Y. Lui, "Magnetotail and Boundary Layer Plasmas at a Geocentric Distance of ~18 R_E: Vela 5 and 6 Observations," *J. Geophys. Res.*, *78*, 7257-7274, 1973.

Asbridge, J.R., S.J. Bame, and I.B. Strong, "Outward Flow of Protons from the Earth's Bow Shock," *J. Geophys. Res.*, *73*, 5777-5782, 1968.

Bame, S.J., J.R. Asbridge, H.E. Felthauser, E.W. Hones, Jr., and I.B. Strong, "Characteristics of the Plasma Sheet in the Earth's Magnetotail," *J. Geophys. Res.*, *72*, 113-129, 1967.

Barfield, J.N., S.E. DeForest, and D.J. Williams, "Simultaneous Observations of Substorm Electrons: Explorer 45 and ATS 5," *J. Geophys. Res.*, *82*, 531-536, 1977.

DeForest, S.E., "Spacecraft Charging at Synchronous Orbit," *J. Geophys. Res.*, *77*, 651-659, 1972.

Fairfield, D.H., "Average and Unusual Locations of the Earth's Magnetopause and Bow Shock," *J. Geophys. Res.*, *76*, 6700-6716, 1971.

Formisano, V., G. Moreno, F. Palmiotto, and P.C. Hedgecock, "Solar Wind Interaction with the Earth's Magnetic Field, 1, Magnetosheath," *J. Geophys. Res.*, *78*, 3714-3730, 1973.

Frank, L.A., "Initial Observations of Low-Energy Electrons in the Earth's Magnetosphere with OGO 3," *J. Geophys. Res.*, *72*, 185-195, 1967a.

Frank, L.A., "On the Extraterrestrial Ring Current During Geomagnetic Storms," *J. Geophys. Res.*, *72*, 3753-3767, 1967b.

Frank, L.A., "Several Observations of Low-Energy Protons and Electrons in the Earth's Magnetosphere with OGO 3," *J. Geophys. Res.*, *72*, 1905-1916, 1967c.

Frank, L.A., "Further Comments Concerning Low-Energy Charged Particle Distributions within the Earth's Magnetosphere and its Environs," in *Particles and Fields in the Magnetosphere*, 319-331, edited by B.M. McCormac, D. Reidel Pub. Co., Dordrecht, The Netherlands, 1970a.

Frank, L.A., "On the Presence of Low-Energy Protons (5 < E < 50 keV) in the Interplanetary Medium," *J. Geophys. Res.*, *75*, 707-716, 1970b.

Frank, L.A., "Plasma in the Earth's Polar Magnetosphere," *J. Geophys. Res.*, *76*, 5202-5219, 1971.

Frank, L.A., K.L. Ackerson, and R.P. Lepping, "On Hot Tenuous Plasma, Fireballs, and Boundary Layers in the Earth's Magnetotail," *J. Geophys. Res.*, *81*, 5859-5881, 1976.

Frank, L.A., and D.A. Gurnett, "Direct Observations of Low-Energy Solar Electrons Associated with a Type III Solar Radio Burst," *Solar Phys.*, *27*, 446-465, 1972.

Frank, L.A. and H.D. Owens, "Omnidirectional Intensity Contours of Low-Energy Protons (0.5 E 50 keV) in the Earth's Outer Radiation Zone at the Magnetic Equator," *J. Geophys. Res.*, *75*, 1269-1278, 1970.

Gringauz, K.I., "Low-Energy Plasma in the Earth's Magnetosphere," *Rev. of Geophys.*, *7*, 339-378, 1969.

Gurnett, D.A., and L.A. Frank, "Continuum Radiation Associated with Low-Energy Electrons in the Outer Radiation Zone," *J. Geophys. Res.*, *81*, 3875-3885, 1976.

Hardy, D.A., J.W. Freeman, and H.K. Hills, "Plasma Observations in the Magnetotail," in *Magnetospheric Particles and Fields*, 89-98, edited by B.M. McCormac, D. Reidel Pub. Co., Dordrecht, The Netherlands, 1976.

Hoffman, R.A., L.J. Cahill, Jr., R.R. Anderson, N.C. Maynard, P.H. Smith, T.A. Fritz, D.J. Williams, A. Konradi, and D.A. Gurnett, "Explorer 45 (S^3 - A) Observations of the Magnetosphere and Magnetopause During the August 4-6, 1972, Magnetic Storm Period," *J. Geophys. Res.*, *80*, 4287-4296, 1975.

Hones, E.W., Jr., J.R. Asbridge, S.J. Bame, M.D. Montgomery, S. Singer, and S.-I. Akasofu, "Measurements of Magnetotail Plasma Flow Made with Vela 4B," *J. Geophys. Res.*, *77*, 5503-5522, 1972.

Hones, E.W., Jr., J.R. Asbridge, S.J. Bame, and S. Singer, "Energy Spectra and Angular Distributions of Particles in the Plasma Sheet and their Comparison with Rocket Measurements over the Auroral Zone," *J. Geophys. Res.*, *76*, 63-87, 1971.

Hones, E.W., Jr., J.R. Asbridge, S.J. Bame, and S. Singer, "Magnetotail Plasma Flow Measured by Vela 4A," *J. Geophys. Res.*, *78*, 5463-5476, 1973.

Hones, E.W., Jr., A.T.Y. Lui, S.J. Bame, and S. Singer, "Prolonged Tailward Flow of Plasma in the Thinned Plasma Sheet Observed at r~18 R_E During Substorms," *J. Geophys. Res.*, *79*, 1385-1392, 1974.

Hundhausen, A.J., "Plasma Measurements across the Bow Shock and in the Magnetosheath" in *Intercorrelated Satellite Observations related to Solar Events*, 155-169, edited by V. Manio, D. Reidel Pub. Co., Dordrecht, The Netherlands, 1970.

Hundhausen, A.J., J.R. Asbridge, S.J. Bame, H.E. Gilbert, and I.B. Strong, "Vela 3 Satellite Observations of Solar Wind Ions: A Preliminary Report," *J. Geophys. Res.*, *72*, 87-100, 1967.

Hundhausen, A.J., S.J. Bame, and J.R. Asbridge, "Plasma Flow Pattern in the Earth's Magnetosheath," *J. Geophys. Res.*, *74*, 2799-2806, 1969.

Hundhausen, A.J., S.J. Bame, J.R. Asbridge, and S.J. Sydoriak, "Solar Wind Proton Properties: Vela 3 Observations from July 1965 to June 1967," *J. Geophys. Res.*, *75*, 4643-4657, 1970.

Lin, R.P., "Non-relativistic Solar Electrons," *Space Sci. Rev.*, *16*, 189-256, 1974a.

Lin, R.P., "Suprathermal Particles," in *Solar Wind 3*, Proceedings of 3rd Solar Wind Conference, 187-194, Pacific Grove, Calif., March 25-29, edited by C.T. Russell, 1974b.

Lin, R.P., K.A. Anderson, and T.L. Cline, "Detection of Interplanetary Electrons from 18 keV to 1.8 MeV during Solar Quiet Times," *Phys. Rev. Lett.*, *29*, 1035-1038, 1972.

Lin, R.P., L.G. Evans, and J. Fainberg, "Simultaneous Observations of Fast Solar Electrons and Type III Radio Burst Emission Near 1 AU," *Astrophys. Lett.*, *14*, 191-198, 1973a.

Lin, R.P., R.E. McGuire, and K.A. Anderson, "Observation of 38-334 keV Interplanetary Protons during Solar Quiet Times," *Phys. Rev. Lett.*, *31*, 1268-1271, 1973b.

Lin, R.P., C.-I. Meng, and K.A. Anderson, "30 to 100 keV Protons Upstream From the Earth's Bow Shock," *J. Geophys. Res.*, *79*, 489-499, 1974.

Lyons, L.R., and D.J. Williams, "The Quiet Time Structure of Energetic (35-560 keV) Radiation Belt Electrons," *J. Geophys. Res.*, *80*, 943-950, 1975.

Lyons, L.R., and D.J. Williams, "Storm-Associated Variations of Equatorially Mirroring Ring Current Protons, 1-800 keV, at Constant First Adiabatic Invariant," *J. Geophys. Res.*, *81*, 216-220, 1976.

Montgomery, M.D., "Average Thermal Characteristics of Solar Wind Electrons," in *Solar Wind*, NASA SP-308, 208-211, edited by C.P. Sonnet, P. J. Coleman, Jr., and J.M. Wilcox, Washington, D.C., 1972.

Montgomery, M.D., J.R. Asbridge, and S.J. Bame, "Vela 4 Plasma Observations Near the Earth's Bow Shock," *J. Geophys. Res.*, *75*, 1217-1231, 1970.

Montgomery, M.D., S.J. Bame, and A.J. Hundhausen, "Solar Wind Electrons: Vela 4 Measurements," *J. Geophys. Res.*, *73*, 4999-5003, 1968.

Ogilvie, K.W., J.D. Scudder, and M. Sugiura, "Electron Energy Flux in the Solar Wind," *J. Geophys. Res.*, *76*, 8165-8173, 1971.

Pizzella, G., and L.A. Frank, "Energy Spectra for Proton (200 eV ≤ E ≤ 1 MeV) Intensities in the Outer Radiation Zone," *J. Geophys. Res.*, *76*, 88-91, 1971.

Reiff, P.H., and D.L. Reasoner, "The Magnetosheath Electron Population at Lunar Distance: General Features," *J. Geophys. Res.*, *80*, 1232-1237, 1975.

Rosenbauer, H., H. Grunwaldt, M.D. Montgomery, G. Paschmann, and N. Sckopke, "Heos 2 Plasma Observations in the Distant Polar Magnetosphere: The Plasma Mantle," *J. Geophys. Res.*, *80*, 2723-2737, 1975.

Sawyer, D.M., and J.I. Vette, "AP-8 Trapped Proton Environment for Solar Maximum and Solar Minimum," NASA-GSFC, Greenbelt, Md., 1976.

Schield, M.A., and L.A. Frank, "Electron Observation between the Inner Edge of the Plasma Sheet and the Plasmasphere," *J. Geophys. Res.*, *75*, 5401-5414, 1970.

Scudder, J.D., D.L. Lind, and K.W. Ogilvie, "Electron Observation in the Solar Wind and Magnetosheath," *J. Geophys. Res.*, *78*, 6535-6548, 1973.

Sears, F.W., *An Introduction to Thermodynamics, the Kinetic Theory of Gases, and Statistical Mechanics*, Addison-Wesley Publishing Co., Cambridge, Mass., 1953.

Singley, G.W., and J.I. Vette, "A Model Environment for Outer Zone Electrons," NASA-GSFC, Greenbelt, Md., 1972.

Smith, P.H., R.A. Hoffman, and T.A. Fritz, "Ring Current Proton Decay by Charge Exchange," *J. Geophys. Res.*, *81*, 2701-2708, 1976.

Stevens, J.R., E.F. Martina, and R.S. White, "Proton Energy Distribution from 0.060 to 3.3 MeV at 6.6 Earth Radii," *J. Geophys. Res.*, *75*, 5373-5385, 1970.

Vasyliunas, V.M., "A Survey of Low-Energy Electrons in the Evening Sector of the Magnetosphere with OGO 1 and OGO 3," *J. Geophys. Res.*, *73*, 2839-2884, 1968.

Vasyliunas, V.M., "Magnetospheric Plasma" in *Solar Terrestrial Physics/1970*, Proc. of the Intern. Symp., Leningrad, U.S.S.R., May 11-19, 1970, edited by E.R. Dyer, D. Reidel Pub. Co., Dordrecht, The Netherlands, 1972.

Vernov, S.N., V.V. Melnikov, I.A. Savenko, and B.I. Savin, "Measurements of Low Energy Particle Fluxes from the Cosmos and Electron Satellites," *Space Res.*, *6*, 746-756, 1966.

Vette, J.I., R.H. Hilberg, and M.J. Teague, "Identification of Satellites Possibly Active During the IMS and Other Orbital Configurations," in *The Scientific Satellite Programme During the International Magnetospheric Study*, 45-59, edited by K. Knott and B. Battrick, D. Reidel Pub. Co., Dordrecht, The Netherlands, 1976.

Wang, J.R., L.A. Fisk, and R.P. Lin, "Observations of the Scatter-Free Solar-Flare Electrons in the Energy Range 20 - 1000 keV," presented at the 12th Intern. Conf. on Cosmic Rays, 65-70, Hobart, Tasmania, Australia, 1971.

Williams, D.J., T.A. Fritz, and A. Konradi, "Observations of Proton Spectra ($1.0 \leq Ep \leq 300$ keV) and Fluxes at the Plasmapause," *J. Geophys. Res.*, *78*, 4751-4755, 1973.

Wolfe, J.H., "The Large-Scale Structure of the Solar Wind," in *Solar Wind*, NASA SP-308, 170-196, edited by C.P. Sonnet, P.J. Coleman, Jr., and J.M. Wilcox, Washington, D.C., 1972.

Wolfe, J.H., and D.S. Intriligator, "The Solar Wind Interaction with the Geomagnetic Field," *Space Sci. Rev.*, *10*, 511-596, 1970.